



OPEN

Unraveling the complex interplay of sex, endocrinology, and inflammation in post-Injury articular cartilage breakdown through in silico modeling

C. Hutcherson^{1,2}, B. Luke³, K. Khader⁴ & Y. Y. Dhaher^{1,2✉}

The onset of degenerative joint diseases such as post-traumatic osteoarthritis (PTOA) are associated with joint injury, biomechanical changes, and synovial biochemical anomalies. Sex and reproductive endocrinology have been emerging as potential risk factors, with epidemiological evidence revealing that female's exhibit higher PTOA risk and poorer outcomes post-injury compared to males. Sex hormones, including estradiol, progesterone, and testosterone, have been shown to regulate inflammatory signaling in immune and synovial cells, yet their collective impact on injury-induced joint inflammation and catabolism is poorly understood. Using an in silico kinetic model, we investigated the effects of sex-specific endocrine states on post-injury mechanisms in the human synovial joint. Our model results reveal that heightened estradiol levels in pre-menopausal females during the peri-ovulatory phase increase interleukin (IL)-1 β expression and suppress IL-10 expression within the synovium after a simulated injury. Conversely, elevated testosterone levels in males decrease post-injury IL-1 β , tumor necrosis factor alpha (TNF)- α , and stromelysin (MMP)-3 expression while increasing IL-10 production compared to females. Gaining insight into the effects of sex hormones on injury-induced inflammation and cartilage degradation provides a basis for designing future experimental and clinical studies to explore their effects on the synovial system, with a particular focus on the female sex.

Post-traumatic osteoarthritis (PTOA) is a form of osteoarthritis that can develop following significant trauma to diarthrodial joints such as the knee and is a leading cause of disability worldwide¹. Epidemiological evidence has identified several risk factors of PTOA, including biomechanical and biochemical abnormalities²; however, it has also been shown that sex differences are associated with PTOA pathogenesis. Specifically, females have been reported to have a higher risk of knee injury^{3,4} and PTOA development^{5–7} compared to males. Previous research efforts have explored the influence of female sex hormones on biomechanical^{8,9} and biological factors^{10–12} affiliated with the onset of PTOA. However, despite an extensive investigation into biomechanical factors, there remains a persistent challenge in characterizing the biological mechanisms influenced by sex hormones responsible for maintaining human joint cartilage homeostasis¹³.

The initiation of joint cartilage degeneration, a hallmark of PTOA onset, is associated with losing the catabolic/anabolic balance between extracellular matrix (ECM) synthesis and degradation¹⁴. Cartilage tissue breakdown is accelerated through elevated pro-inflammatory cytokine levels, triggering the increased synthesis of catabolic enzymes from the group of matrix metalloproteinases (MMPs), mainly collagenase 1 (MMP-1), stromelysin 1 (MMP-3), gelatinase B (MMP-9) and collagenase 3 (MMP-13) from cells that reside within the synovium^{15,16}. Prior research has highlighted the impact of sex hormones, particularly estradiol, progesterone, and testosterone, on the production of MMPs through the modulation of inflammatory signaling pathways^{17–19}. In experimental studies, progesterone and testosterone have been shown to promote anti-inflammatory signaling by modulating pathways associated with cytokines such as interleukin (IL)-10 in immune cells^{17,20}. However, research has shown complex biological effects linked to the primary sex hormone, estradiol, which

¹Department of Physical Medicine and Rehabilitation, University of Texas Southwestern, Dallas, TX, USA.

²Department of Orthopaedic Surgery, University of Texas Southwestern, Dallas, TX, USA. ³Department of Mechanical Engineering, Valparaiso University, Valparaiso, IN, USA. ⁴Division of Epidemiology, Department of Internal Medicine, University of Utah, Salt Lake City, UT, USA. ✉email: Yasin.Dhaher@UTSouthwestern.edu

can vary depending on cell type and concentration^{12,19}. For instance, elevated doses of estradiol observed in females during late pregnancy have been shown to elicit anti-inflammatory and anabolic effects on immune cells^{21,22}, synoviocytes^{23,24} and chondrocytes^{25,26}. Conversely, levels of estradiol associated with early follicular to peri-ovulatory phases have been reported to induce pro-inflammatory effects in immune cells, particularly monocytes/macrophages^{19,27}.

Notably, synovial fluid (SF) estradiol concentrations in pre-menopausal females fall within a range shown to increase pro-inflammatory effects in macrophages in animal model systems, particularly impacting pathways associated with the production of IL-1 β and TNF- α ^{19,28}. As a result, circulating estradiol levels in pre-menopausal women, particularly during stages of increased expression such as the peri-ovulation period (cycle day 12–14) and late luteal phase (cycle day 24–26) of the menstrual cycle (refer to Fig. 1 for a graph of the female menstrual cycle), may disrupt the catabolic/anabolic balance within the synovial joint following a traumatic injury, potentially leading to unfavorable post-injury outcomes.

Unfortunately, due to the inherent complexity of monitoring the acute biological process after joint trauma, our ability to investigate the modulatory role of sex hormones on biological factors involved with synovial tissue catabolism is limited through traditional experimentation. Thus, a complementary *in silico* approach could present a unique advantage by providing a targeted and time-efficient analysis of this inaccessible biological

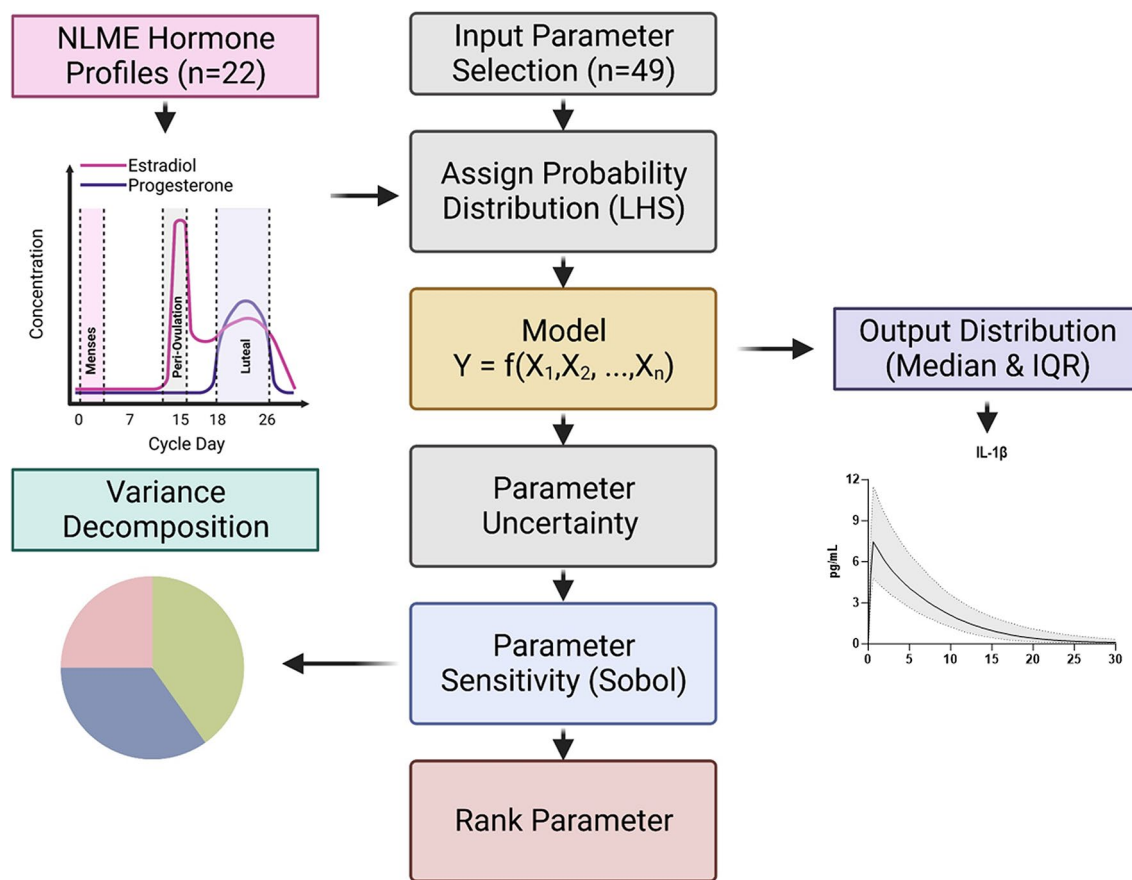


Fig. 1. Summary of the model process. Estimation of nominal parameters and sex hormone profiles. The first step in the modeling process was to estimate the nominal production and clearance rate coefficients ($n=49$) from published *in vitro* studies (cited in Table S3). Additionally, a harmonic nonlinear model mixed effects model fits the mean and standard deviation interval of blood serum hormone data collected from 22 female subjects²⁹. Latin Hypercube Sampling We varied the input parameters between 40 and 160% ($\pm 60\%$) of their nominal values. Hormone concentrations where also varied between maximum and minimum of the NLME generated mean values at each day of the menstrual cycle. We selected a set of input parameters and hormone concentrations within the sampled matrices to solve the differential equations. After solving the equations with all 1000 randomly varied sets of inputs, we determined the median and interquartile range of the outputs at every time point for the modeled substances, generating the likelihood time responses for concentration under parametric uncertainties—sobol sensitivity analysis. We used Sobol's decomposition method to analyze the output data³⁰. The total output variance for each substance was decomposed to determine individual input parameters' contributions and interactions with other inputs. It is used to compute first-order and total-order indices. Variables with higher Sobol sensitivity indices have a more significant impact on the output, while those with lower indices have less influence. The top 5 ranked inputs were determined at each simulated time step for every modeled substance—figure created with BioRender.com.

system using existing in vitro data^{31,32}. In the context of joint health, in silico models analyzing post-injury biological mechanisms are scarce, with only two prior models being proposed by Baker et al.³³ and by our group³⁴. Our previously published mathematical model was designed to break down the various kinetic interactions of cytokines and MMPs after a simulated injury to the joint and to determine the relative contribution of sex-specific endocrinological factors on the response. While our previous model captured salient features of the post-injury synovial inflammatory cascade under sex-specific hormonal conditions, the framework did not include the biological contributions from articular chondrocytes. This was primarily attributed to the relatively lacking in vitro examinations focused on basic chondrocyte molecular kinetics in the presence and absence of sex hormones^{32,34}. Additionally, our prior construct did not account for the impact of physiological changes in sex hormone concentrations throughout the female menstrual cycle on the post-injury metabolic response.

Thus, in this present work, we sought to further improve the viability of our *in-silico* framework by incorporating the contribution of articular chondrocytes and to characterize further the contribution of female sex hormones generated from human subjects on the post-injury catabolic response within the synovial joint. We hypothesize that (1) the increased presence of the female sex hormone estradiol during the peri-ovulatory phase of the menstrual cycle will increase the magnitude of pro-inflammatory cytokine production after a simulated injury, which in turn will increase the production of MMPs, while (2) elevated concentrations of the predominately male sex hormone testosterone will stimulate increased production of anti-inflammatory cytokines, inhibiting the cellular expression of MMPs. This quantitative framework is helpful for future investigations of endocrine-driven molecular mechanisms that influence the synovial microenvironment. Furthermore, the insights gained from this model can serve as valuable guidance for research initiatives to mitigate or prevent post-injury articular cartilage destruction caused by PTOA, with a particular focus on females.

Results

Establishing model initial conditions

Table 1 presents the model equations formulated for each molecular substance (refer to Eq. 1 in methods for a detailed breakdown of the model equations), along with the initial conditions resulting from a simulation conducted without an inflammatory stimulus. This simulation involved only synovial fibroblasts and chondrocytes, without macrophages. In Table 1, the model's initial condition outputs are presented alongside experimentally reported concentrations for each molecule obtained from SF aspirate from healthy or non-injured (contralateral) human knees. The modeled concentrations for IL-1 β [Median (75% Quartile (Q3)—25% Quartile (Q1); 0.040 (0.057–0.028) pg/mL], TNF- α [0.18 (0.27–0.13) pg/mL], IL-6 [19.91 (28.70–14.00) pg/mL], IL-10 [0.44 (0.66–0.31) pg/mL], and MMP-3 [98.08 (151.40–64.02) ng/mL] at the healthy steady state were found to be within the range of reported healthy human SF concentrations. Discrepancies were noted in the modeled values for TIMP-1 [254.80 (367.88–195.94) ng/mL] and MMP-1 [12.66 (20.40–8.55) ng/mL], resulting in over two-fold differences from the reported human SF levels of these molecules. However, the model values fell within the reported SF concentration ranges for these substances. Larger discrepancies were observed for TGF- β [5.83 (8.80–3.90) pg/mL], MMP-9 [0 ng/mL], and MMP-13 [3.07 (4.437–2.21) ng/mL], where our modeled initial conditions values fell outside the reported ranges of these molecules in human SF.

Nonlinear mixed effects fitting of human female sex hormone profiles

Figure 2 displays the profiles of estradiol, progesterone, and testosterone obtained from the mixed-effects model with harmonic terms on serum data collected in 22 healthy female subjects²⁹. A summary of the population demographics is provided in Table S1. The mean and standard deviation (SD) of the concentrations of estradiol at key menstrual cycle time points were as follows: 44.7 ± 15.4 pg/mL on the first day of menses (cycle day 1), 315.2 ± 92.4 pg/mL during peri-ovulation (cycle day 15), and 145.8 ± 40.28 pg/mL at late luteal (cycle day 26). The corresponding progesterone concentrations at those time points were 1.1 ± 0.6 ng/mL, 0.5 ± 0.4 ng/mL, and 7.84 ± 3.05 ng/mL, respectively. For testosterone, the concentrations were reported as 30.6 ± 13.3 ng/dL, 42.9 ± 16.6 ng/dL, and 32.1 ± 12.4 ng/dL, respectively. Notably, these modeled concentrations fall within the reported range of female sex hormone concentrations found in the literature^{35,36}.

Verification of the model outputs

Figure 3 illustrates the synovial concentrations of IL-1 β , TNF- α , IL-6, IL-10, MMP-1, MMP-3, MMP-9, and MMP-13 derived from our LHS analysis (without considering sex hormones). These concentrations were overlaid with independent *in vivo* human experimental findings throughout the simulation^{37–40}. Human SF concentrations of IL-1 β [Mean \pm SD; 4.80 ± 1.69 pg/mL], TNF- α [4.50 ± 2.94 pg/mL], and IL-10 [15.22 ± 12.30 pg/mL] reported by Irie et al.³⁷ one day post joint injury where within the projected range of our modeling results [Median (Q3–Q1); IL-1 β : 7.16 (11.10–4.59) pg/mL; TNF- α : 9.65 (14.80–5.81) pg/mL; IL-10: 17.90 (28.20–11.50)]. Although our modeled concentrations of IL-6 [453.88 (726.33–288.99) pg/mL] were elevated compared to SF data reported by Irie et al.³⁷ one day post-injury [22.00 ± 15.29 pg/mL], human SF concentrations of IL-6 reported by Watt et al.³⁸ [1359.12 (3127.13–628.75) pg/mL] two days post-injury were found to be notably elevated compared to our model results [336.68 (532.97–212.22) pg/mL] as well as Irie et al.³⁷. However, in the later portion of our model simulation for IL-6 at 22 days post injury, the *in vivo* data reported by Watt et al.³⁸ [32.70 (56.89–20.45) pg/mL] was within the range of our modeling results [29.21 (47.18–19.19) pg/mL]. Moreover, MMP-1 [53.250 (85.960–32.99) ng/mL], MMP-3 [390.62 (575.39–265.18) ng/mL], and MMP-9 [6.52 (11.03–3.86) ng/mL] human SF levels reported one day post-injury from Haller et al.³⁹ where within the range of our model projections [MMP-1: 35.38 (53.47–23.42) ng/mL; MMP-3: 288.72 (432.22–4195.81) ng/mL; MMP-9: 7.36 (11.60–4.57) ng/mL], while MMP-13 was slightly decreased compared to our model projections.

Modeled substance	Median healthy initial value (IQR)	Concentration reported in healthy human SF	Subject number	References	Equation
IL-1 β^*	0.040 (0.029) $\frac{\text{pg}}{\text{ml}}$	$1 \pm 2 \frac{\text{pg}}{\text{ml}}$	20	⁴²	$\begin{aligned} \frac{dC_{IL1}}{dt} = & k_{IL1,M1}g_{IL10,IL1}q_{TGF,IL1}(1+f_{E2,IL1})(1+f_{IL6,IL1})C_{M1} \\ & +k_{IL1,M2}C_{M2}+k_{IL1,SF}(1+f_{TNF,IL1SF})(1+f_{IL1,IL1SF})C_{SF} \\ & +k_{IL1,CH}(1+f_{TNF,IL1CH})C_{CH}-k_{d,IL1}C_{IL1} \end{aligned}$
TNF- α	0.18 (0.13) $\frac{\text{pg}}{\text{ml}}$	2.21 (2.85) $\frac{\text{pg}}{\text{ml}}$	20	⁴⁰	$\begin{aligned} \frac{dC_{TNF}}{dt} = & k_{TNF,M1}g_{IL10,TNF}q_{TGF,TNF}g_T,TNFg_P,TNF \\ & (1+f_{FNF,TNF})(1+f_{IL6,TNF})C_{M1}+k_{TNF,M2}C_{M2} \\ & +k_{TNF,SF}(1+f_{IL1,TNF})C_{SF}+k_{TNF,CH}C_{CH}-k_{d,TNF}C_{TNF} \end{aligned}$
IL-6****	19.91 (14.7) $\frac{\text{pg}}{\text{ml}}$	21.0 [1.1–41.3] $\frac{\text{pg}}{\text{ml}}$	72	⁴⁶	$\begin{aligned} \frac{dC_{IL6}}{dt} = & k_{IL6,M1}g_{IL10,IL6}q_{E2,IL6}(1+f_{TGF,IL6})C_{M1} \\ & +k_{IL6,M2}C_{M2}+k_{IL6,SF}(1+f_{IL1,IL6SF})(1+f_{TNF,IL6SF})C_{SF} \\ & +k_{IL6,CH}(1+f_{TNF,IL6CH})(1+f_{IL1,IL6CH})C_{CH}-k_{d,IL6}C_{IL6} \end{aligned}$
IL-10*	0.439 (0.35) $\frac{\text{pg}}{\text{ml}}$	$1 \pm 6 \frac{\text{pg}}{\text{ml}}$	20	⁴²	$\begin{aligned} \frac{dC_{IL10}}{dt} = & k_{IL10,M1}q_{E2,IL10}(1+f_{TGF,IL10}) \\ & (1+f_{T,IL10})(1+f_{IL6,IL10})C_{M1}+k_{IL10,M2}C_{M2} \\ & +k_{IL10,SF}C_{SF}+k_{IL10,CH}C_{CH}-k_{d,IL10}C_{IL10} \end{aligned}$
TGF- β^{**}	5.83 (4.90) $\frac{\text{pg}}{\text{ml}}$	N.D	7	⁸¹	$\begin{aligned} \frac{dC_{TGF}}{dt} = & k_{TGF,P}C_P+k_{TGF,M1}C_{M1} \\ & +k_{TGF,M2}C_{M2}+k_{TGF,SF}(1+f_{TNF,TGFSF})C_{SF} \\ & +k_{TGF,CH}(1+f_{IL6,TGFCH})(1+f_{IL1,TGFCH})C_{CH}-k_{d,TGF}C_{TGF} \end{aligned}$
TIMP-1*	254.8 (1719) $\frac{\text{ng}}{\text{ml}}$	124 (416.22) $\frac{\text{ng}}{\text{ml}}$	25	⁴⁴	$\begin{aligned} \frac{dC_{TIMP1}}{dt} = & k_{TIMP1,M1}g_{TNF,TIMP1}g_{IL1,TIMP1a}g_{IL10,TIMP1}C_{M1} \\ & +k_{TIMP1,M2}C_{M2}+k_{TIMP1,SF}(1+f_{TNF,TIMP1SF})C_{SF} \\ & (1+f_{IL1,TIMP1SF})C_{SF}+k_{TIMP1,CH} \\ & (1+f_{TGF,TIMP1CH})g_{IL1,TIMP1CH}C_{CH}-k_{d,TIMP1}C_{TIMP1} \end{aligned}$
MMP-1*	12.66 (1185) $\frac{\text{ng}}{\text{ml}}$	3.66 (58.42) $\frac{\text{ng}}{\text{ml}}$	13	⁴³	$\begin{aligned} \frac{dC_{MMP1}}{dt} = & k_{MMP1,M1}C_{M1}+k_{MMP1,SF} \\ & (1+f_{TNF,MMP1SF})(1+f_{IL1,MMP1SF})C_{SF} \\ & +k_{MMP1,CH}(1+f_{IL6,MMP1CH})(1+f_{IL1,MMP1CH})C_{CH}-k_{d,MMP1}C_{MMP1} \end{aligned}$
MMP-3	98.08 (8738) $\frac{\text{ng}}{\text{ml}}$	164.29 [126.23–202.34] $\frac{\text{ng}}{\text{ml}}$	72	⁴⁶	$\begin{aligned} \frac{dC_{MMP3}}{dt} = & k_{MMP3,SF}(1+f_{TNF,MMP3SF}) \\ & (1+f_{IL1,MMP3SF})(1+f_{IL6,MMP3SF})C_{SF}+k_{MMP3,CH}(1+f_{IL1,MMP3CH}) \\ & (1+f_{IL6,MMP3CH})C_{CH}-k_{d,MMP3}C_{MMP1} \end{aligned}$
MMP-9***	0 $\frac{\text{pg}}{\text{ml}}$	$14.9 \pm 2.2 \frac{\text{pg}}{\text{ml}}$	120	⁴⁷	$\begin{aligned} \frac{dC_{MMP9}}{dt} = & k_{MMP9,M1}g_{IL10,MMP9}(1+f_{IL1,MMP9})(1+f_{TNF,MMP9})C_{M1} \\ & +k_{MMP9,M2}C_{M2}-k_{d,MMP9}C_{IL1} \end{aligned}$
MMP-13	3.071 (2.23) $\frac{\text{ng}}{\text{ml}}$	$0.012 \pm 0.002 \frac{\text{ng}}{\text{ml}}$	120	⁴⁷	$\begin{aligned} \frac{dC_{MMP13}}{dt} = & k_{MMP13,SF}(1+f_{TNF,MMP13SF})C_{SF} \\ & +k_{MMP13,CH}(1+f_{IL1,MMP13CH}) \\ & (1+f_{IL6,MMP13CH})C_{CH}-k_{d,MMP13}C_{MMP13} \end{aligned}$

Table 1. Initial values and equations for modeled substances (plausibility of our estimates). IQR: Interquartile range; SF: Synovial fluid; \pm : Reported mean and standard deviation; (): Reported median and IQR; []: Reported mean and 95% confidence interval; N.D: Non detectable levels of molecules in healthy human SF. All studies included in the table measured SF protein levels in healthy or non-injured contralateral control knee using enzyme-linked immunosorbent assay techniques. *In some cases, the margin of error for the measurements extended below a concentration of 0 pg/mL, suggesting that the experimental data may have been non-normally distributed, may have had extreme outliers, or may have been averaged over a small number of samples. However, very few studies report concentrations of cytokines in healthy joints, and the ones cited here serve as a starting point for comparisons. **TGF- β in this study was reported to be below assay detection range of 7 pg/ml, which encompasses our model estimate. Furthermore, other human studies have also reported low or absent TGF- β values in healthy SF⁴¹. TGF- β has been reported for post-injury joints⁷³, however, data on independent healthy controls in these studies were not reported. ***Our estimate of initial MMP-9 concentration is lower than the concentration reported in a non-injured contralateral knee (a common control). However, this will lead to a conservative estimate of its concentration once an inflammatory stimulus is included in the model. Note that other examinations for MMP-9 in healthy and non-injured contralateral control knees indicate large variability in the data. For example, in 12 subjects, Iverson et al.⁸⁴ reported SF MMP-9 levels at 122.50 (4300.56) pg/mL in non-injured contralateral knees. Our prediction of the initial value for MMP-9 concentration in the SF is plausible given the literature. ****IL-6 reported in healthy contralateral joints. Note that other examinations for IL-6 using contralateral limb as a healthy control report a range 3.8 ± 2.9 on 120 subjects⁴⁷ indicating large variability across studies. Our prediction of the initial value for IL-6 concentration in the SF is plausible given the literature.

While continuous in vivo time-course data is limited for the substances encompassed by our model, we incorporated several pertinent discrete in vivo datasets reporting the SF levels of the included molecules at distinct time points within 30 days post-injury, as presented in Table S2 and in our previous work³⁴.

Variance-based sensitivity analysis

We conducted 100,000 iterations of our model to assess the influence of production and clearance inputs on the modeled output variance over the entire simulation duration for each substance. On each day post-injury

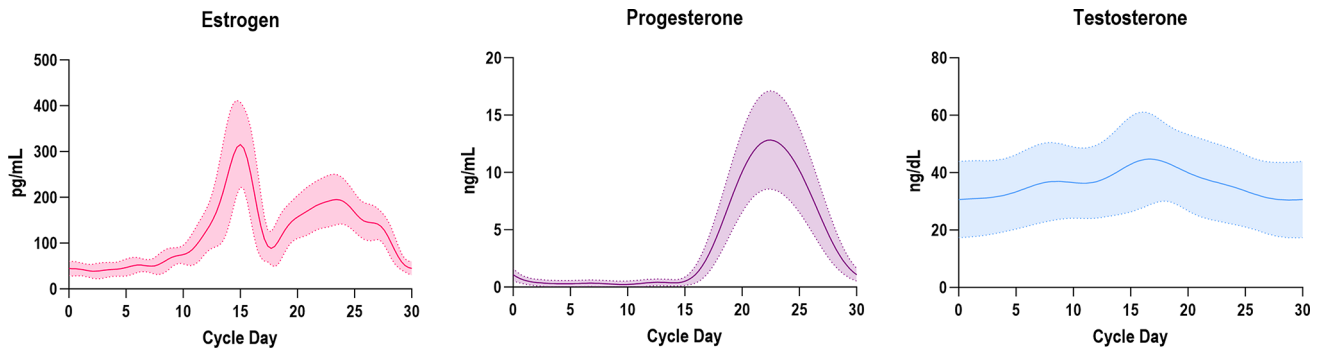


Fig. 2. Menstrual hormonal profiles from healthy female subjects fitted using harmonic NLME fitting. Cycle day 0 corresponds to the onset of menses, 15 to the peak of estradiol concentration (peri-ovulatory cycle phase), 23 to the zenith of progesterone levels (luteal cycle phase), and 30 to the final day of the cycle. The solid line illustrates the collective mean serum hormone concentrations of all 22 female subjects, while the shaded area represents the standard deviation. Figure created using GraphPad Prism version 10.2.2 for Windows, GraphPad Software, Boston, Massachusetts USA, <https://www.graphpad.com>.

(simulation days 1–30), we computed the first-order Sobol sensitivity values for random varied parameter sets, ranking the top five most sensitive parameters. The ranked averaged first-order sensitivity indices for varied parameters linked to IL-1 β , TNF- α , IL-6, IL-10, MMP-1, MMP-3, MMP-9, and MMP-13 are presented in a heatmap format in Fig. 4, spanning the simulation duration.

We showed that varied efflux parameters in our model assigned to IL-1 β ($k_{IL1\beta d}$), TNF- α ($k_{TNF\alpha d}$), IL-6 ($k_{IL6 d}$), IL-10 ($k_{IL10 d}$), and MMP-9 ($k_{MMP9 d}$) yielded the top first order sensitivity rank from simulation day 1–7, contributing to [Mean \pm SD] $38.7 \pm 2.1\%$ (IL-1 β), $32.0 \pm 4.9\%$ (TNF- α), $35.6 \pm 1.3\%$ (IL-6), $33.6 \pm 5.1\%$ (IL-10), and $32.0 \pm 5.4\%$ (MMP-9) of the output variance respectively. Varied M1 macrophage production parameters contributed to $28.4 \pm 3.6\%$ of modeled output variance for IL-1 β ($k_{IL1\beta M1}$) and $21.1 \pm 3.9\%$ for TNF- α ($k_{TNF\alpha M1}$), while M1 macrophage influx parameters (k_{M1in}) contributed to $24.8 \pm 3.0\%$ of the output variance for IL-6, $22.3 \pm 7.0\%$ for IL-10 and $26.1 \pm 6.1\%$ for MMP-9, ranking second during this simulation period. Beyond simulation day 7, we observed a transition in the first-ranked sensitive parameters for these substances. Specifically, the first-order sensitivity indices associated with macrophage efflux parameters ($k_{m d}$) ranked first for IL-1 β , TNF- α , IL-6, IL-10, and MMP-9, contributing to $47.9 \pm 11.8\%$ (IL-1 β), $44.3 \pm 7.2\%$ (TNF- α), $38.3 \pm 5.6\%$ (IL-6), $50.4 \pm 6.0\%$ (IL-10), and $49.4 \pm 6.7\%$ (MMP-9) of output variance these substances until the conclusion of the simulation.

Varied efflux parameters for MMP-1 ($k_{MMP1 d}$), MMP-3 ($k_{MMP3 d}$), and MMP-13 ($k_{MMP13 d}$) were ranked first across the entire simulation duration, contributing to $48.1 \pm 3.0\%$ (MMP-1), $51.8 \pm 3.6\%$ (MMP-3), and $62.7 \pm 3.6\%$ (MMP-13) of the modeled output variances for these substances. Varied chondrocyte production parameters contributed to $26.9 \pm 3.4\%$ of the output variance for MMP-1 ($k_{MMP1 CH}$) and $40.1 \pm 4.3\%$ for MMP-3 ($k_{MMP3 CH}$), and synovial fibroblast production parameters contributed to $26.4 \pm 2.1\%$ of the output variance for MMP-13 ($k_{MMP13 SF}$) ranking as second for these substances at all simulation time points.

Female endocrine analysis

Figure 5 depicts the impact of initiating the injury model at different time points during the female menstrual cycle on both the projected post-injury response (Fig. 5A,C) and the maximum model output (Fig. 5B,D) for IL-1 β , TNF- α , IL-6, IL-10, MMP-1, MMP-3, MMP-9, and MMP-13. To accurately represent the female endocrine state in our simulations, we integrated hormone levels from NLME group representative profiles for estradiol, progesterone, and testosterone in pre-menopausal females (Fig. 2). All model simulation parameters were varied $\pm 20\%$ for 1000 iterations using LHS to accommodate biological variations in input parameters. Sex hormone inputs were also randomly varied for each model iteration within the established range of values from the NLME group profiles. The maximum substance output across each model iteration was calculated for each group. The distribution of these maximum output values was analyzed using rank-based covariate adjustment methods (RBC; see methods for more details). Dunn's multiple comparisons test was conducted on adjusted output data from injury simulations initiated at various menstrual phases: menses (cycle day 0), mid-follicular (cycle day 7), peri-ovulatory (cycle day 15), early luteal (cycle day 18), and late luteal (cycle day 26). Statistical significance for group comparisons was adjusted using Šidák correction to 0.0051 from 0.05.

Our simulations revealed that the projected maximum post-injury expression of IL-1 β was significantly elevated when the injury model was initiated at peri-ovulation [Median (Q3-Q1); 17.80 (27.70–11.40) pg/mL] compared to when the injury model was initiated at menses [10.60 (16.30–6.80) pg/mL, $p < 0.001$], mid follicular [11.20 (17.30–7.20) pg/mL, $p < 0.001$], early luteal [13.70 (21.30–8.80) pg/mL, $p < 0.001$], and late luteal [15.30 (23.40–9.50) pg/mL, $p < 0.001$] endocrine states. Moreover, the maximum post-injury expression of IL-1 β when injury was induced at peri-ovulation and at early and late luteal states were significantly increased compared to menses, an endocrine muted state [$p < 0.001$].

Interestingly, when the injury model was initialized during peri-ovulation, maximum IL-10 output [23.13 (36.39–14.97) pg/mL] significantly decreased compared to the mid follicular [26.86 (41.52–15.56) pg/mL,

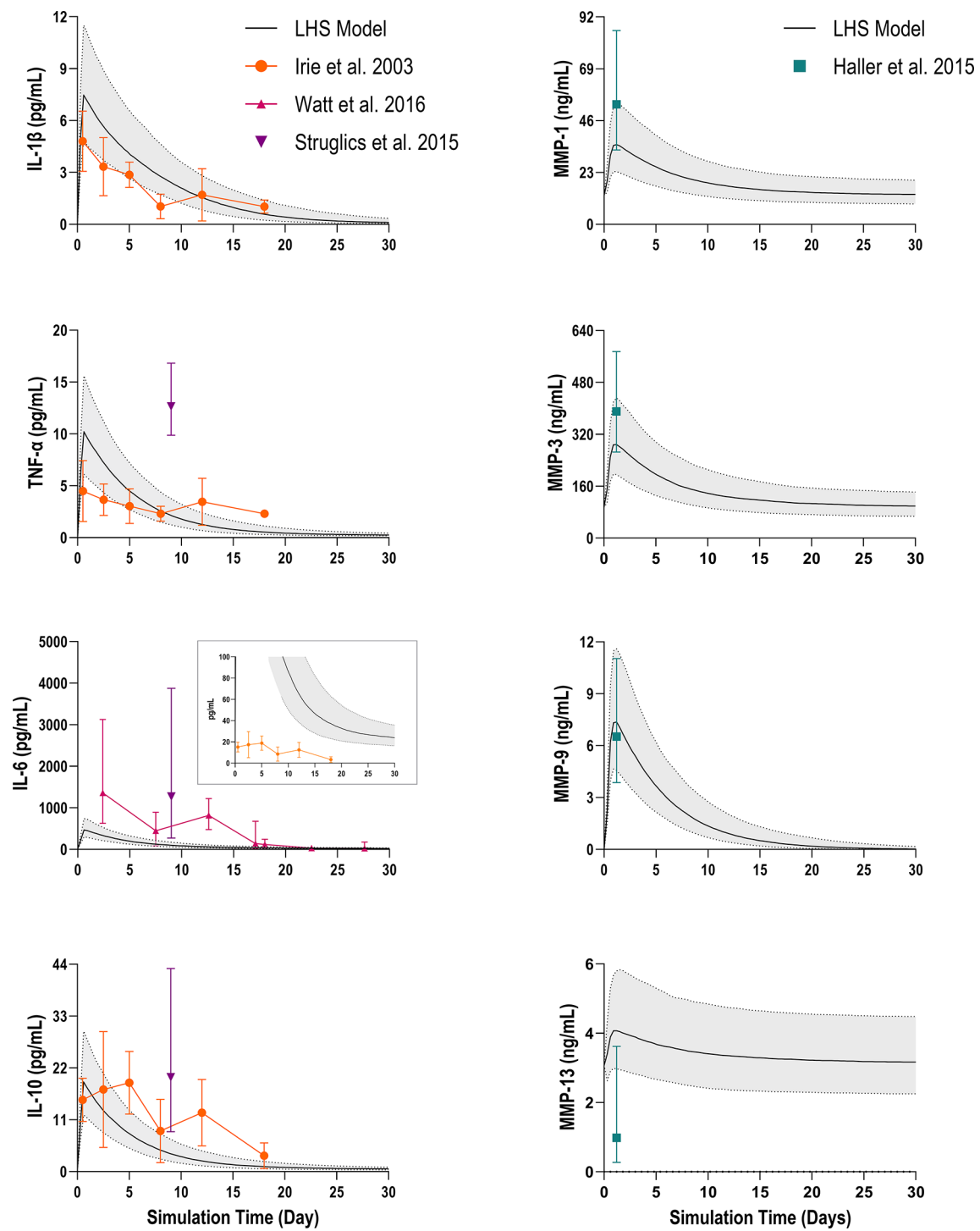


Fig. 3. Model results for LHS analysis of IL-1 β , TNF- α , IL-6, IL-10, MMP-1, MMP-3, MMP-9, and MMP-13 (Median \pm IQR) compared to independent in vivo synovial concentrations following joint injury^{37–40}. Simulation results for each molecule shown as median (solid black lines) \pm IQR (gray bands). Continuous in vivo comparison data from Irie et al. 2003 (ACL injury; 24 h ($n=5$), 2–3 days ($n=14$), 4–6 days ($n=5$), 7–9 days ($n=5$), 10–14 days ($n=4$), 15–21 days ($n=3$)) are shown as orange circles with error bars and from Watt et al. 2016 (acute knee injury; baseline (1–17 days) ($n=136$), 14 day visit ($n=83$), 3 month visit ($n=14$)) with pink upward triangle with error bars. Discrete data from Struglics et al. 2015 (ACL injury; 0–6 weeks ($n=47$)) are shown with purple downwards triangles with error bars, and from Haller et al. 2015 (articular fracture; < 24 h ($n=45$)) with blue squares with error bars. See Table S2 for independent comparisons of the model's remaining molecules. The figure was created using GraphPad Prism version 10.2.2 for Windows, GraphPad Software, Boston, Massachusetts USA, www.graphpad.com.

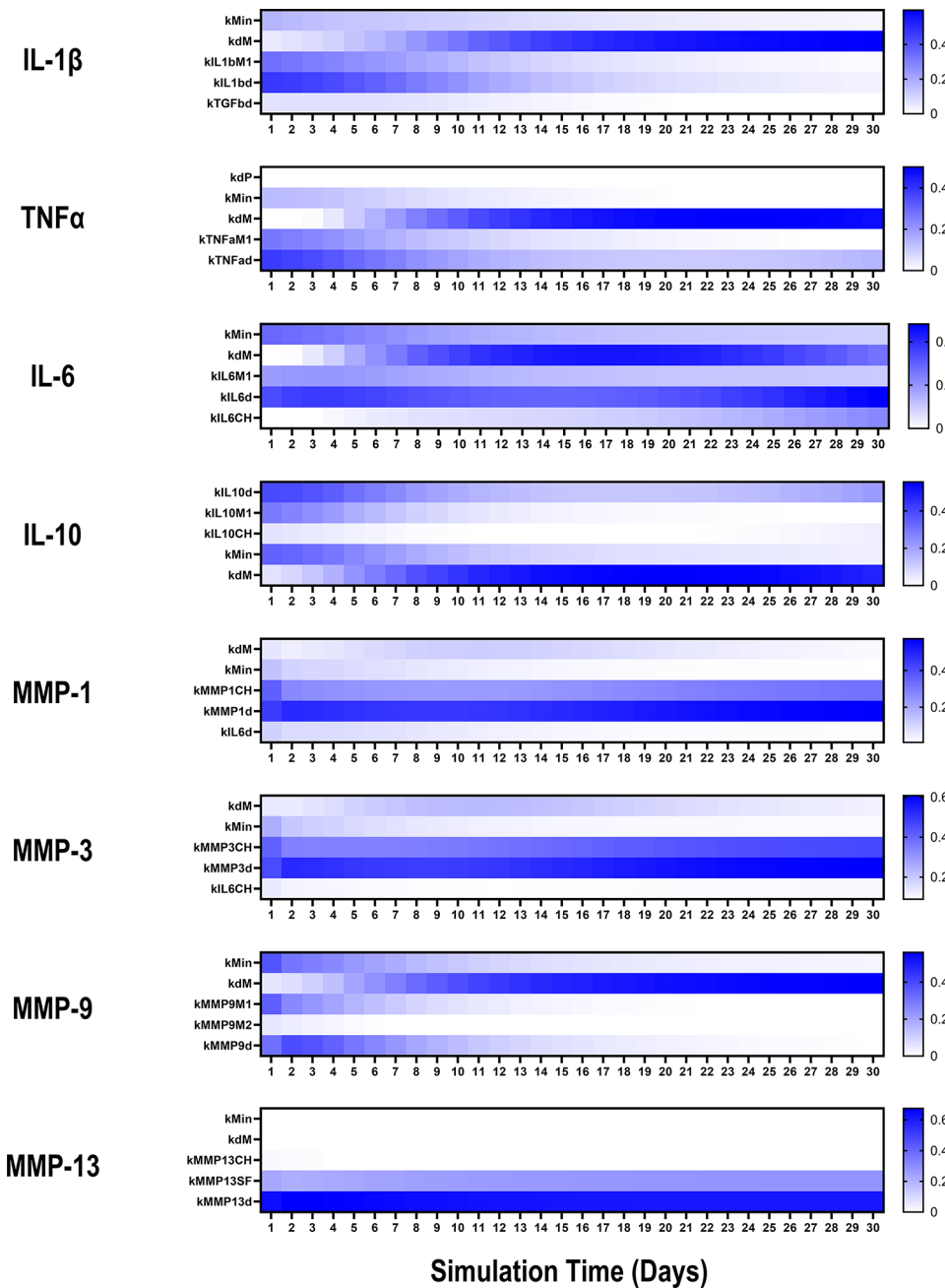


Fig. 4. First-Order Sensitivity Analysis Results for input parameters associated with IL-1 β , TNF- α , IL-6, IL-10, MMP-1, MMP-3, MMP-9, and MMP-13. The calculated first-order sensitivity values for each input parameter ($n=49$) were averaged and ranked on a scale of 1 to 5, then presented in a heat map format for each modeled output. This heat map visually illustrates the time-dependent influence of the top 5 ranked input parameters throughout the simulation duration. A detailed description of each input parameter can be found in Table S3. In the heat map, blue shading indicates higher sensitivity values at the simulated time point, while white shading indicates lower sensitivity values. Figure created using GraphPad Prism version 10.2.2 for Windows, GraphPad Software, Boston, Massachusetts USA, <https://www.graphpad.com>.

$p < 0.001$] and early luteal phases of the menstrual cycle [25.60 (40.43–16.45) pg/mL, $p = 0.003$]. Maximum IL-10 levels at peri-ovulation also trended lower than the maximum output at menses [26.23 (40.43–15.99) pg/mL, $p = 0.007$].

Changes in female sex hormones during the menstrual cycle at the time of injury did not impact the projected maximum expression of TNF- α , IL-6, TGF- β , MMP-1, MMP-3, MMP-9, MMP-13, and TIMP-1 in this study.

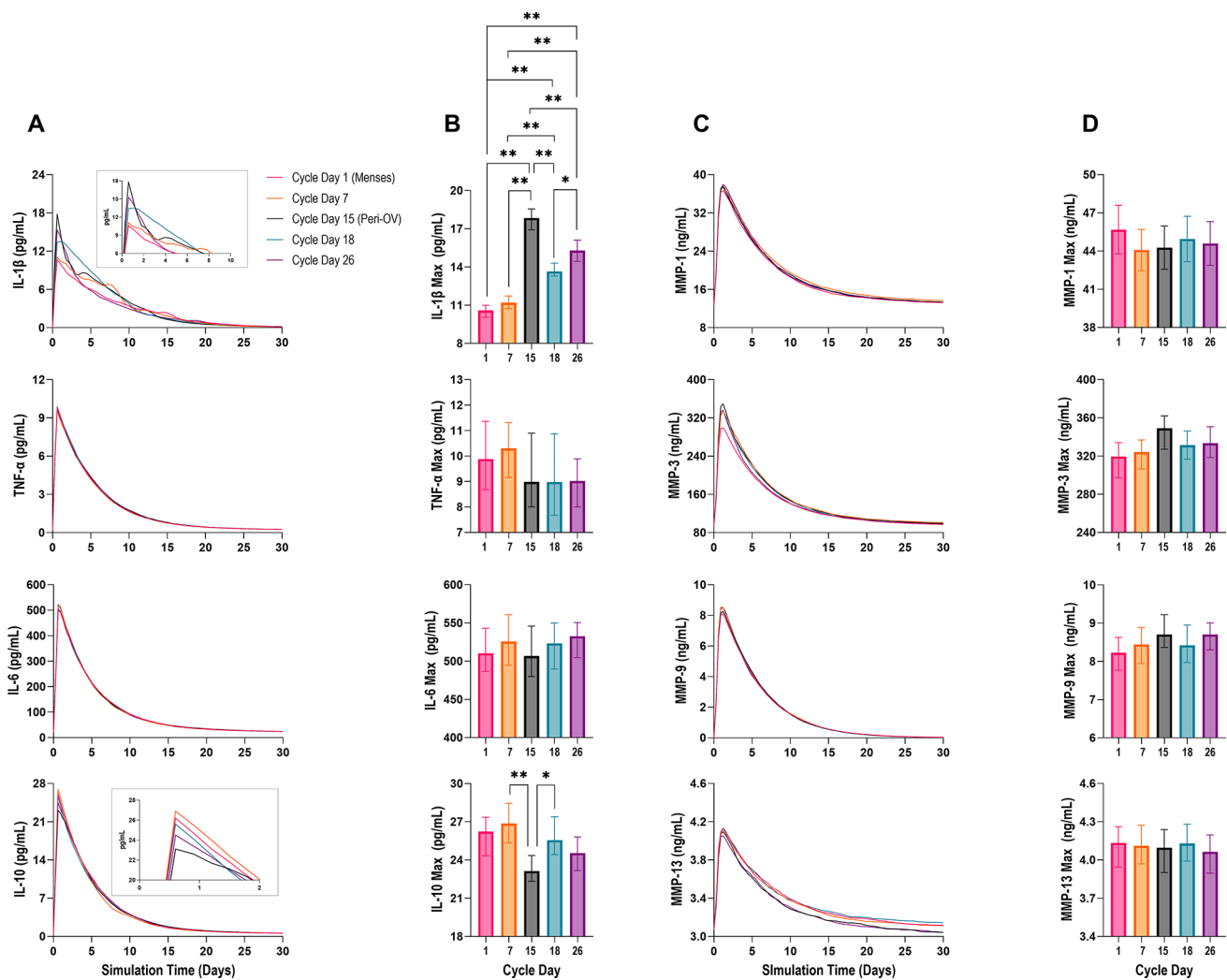


Fig. 5. Effects of combined sex hormones at physiological levels during the female menstrual cycle. Menstrual sweep model results for (A) IL-1 β , TNF- α , IL-6, IL-10, (C) MMP-1, MMP-3, MMP-9, and MMP-13 (Median). LHS model results are presented based on simulations initiated at each day of the menstrual cycle, accounting for variations in sex hormone concentrations and utilizing menstrual hormone profiles generated from NLME fitting. The model's outputs are depicted over time for each molecule under key sex hormone conditions: menses (cycle day 1, pink line), mid follicular (cycle day 7, orange line), peri-ovulatory (cycle day 15, black line), early luteal (cycle day 18, blue line), and late luteal (cycle day 26, purple line). Magnified regions were added for IL-1 β and IL-10 to better visualize menstrual hormonal effects on the early post injury response. Maximum modeled concentrations for (B) IL-1 β , TNF- α , IL-6, IL-10, (D) MMP-1, MMP-3, MMP-9, and MMP-13 at each female menstrual condition (Median \pm 95% CI). The median and IQR of maximum concentrations were derived from LHS modeling results with simulations initiated at key endocrine states during the female menstrual cycle. Comparisons of the maximum outputs distribution for the substances at each of the simulated endocrine states were conducted using RBC methods and Dunn's multiple comparison post hoc test—statistical significance after Šidák correction was set to $p = 0.0051$. Stars indicate significance ($p < 0.0051 = ^*$, $p < 0.0001 = ^{**}$). Figure created using GraphPad Prism version 10.2.2 for Windows, GraphPad Software, Boston, Massachusetts USA, <https://www.graphpad.com>.

Sex dimorphism analysis

Figure 6 illustrates the model output distributions for IL-1 β , TNF- α , IL-6, IL-10, MMP-1, MMP-3, MMP-9, and MMP-13, considering simultaneous variations in input parameters and sex hormone profiles for male and female endocrine states (menses and peri-ovulatory) using LHS. The distribution of these outputs was analyzed using RBC methods. Dunn's multiple comparisons were performed on the output distributions of male and female peri-ovulation and menses injury models for each simulation day (simulation day 1–30) using a Šidák-adjusted significance level of 0.017.

Simulations under the male endocrine condition resulted in significantly inhibited model output distributions for IL-1 β [simulation day 1–14, $p < 0.001$] and MMP-3 [simulation day 1, $p = 0.001$], while elevating IL-10 [simulation day 1–11, $p < 0.001$] compared to female peri-ovulatory simulations. Conversely, compared to the

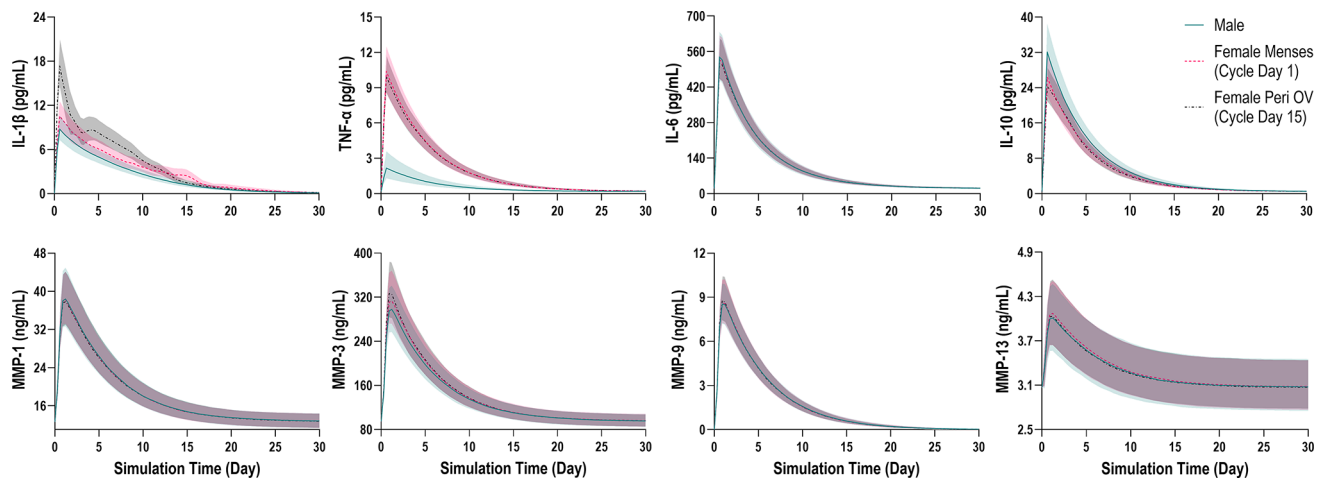


Fig. 6. Effects of combined sex hormones at physiological levels for males and females on the output distribution for IL-1 β , TNF- α , IL-6, IL-10, MMP-1, MMP-3, MMP-9, and MMP-13 (Median \pm IQR). Blue: model output distribution for simulations incorporating sex hormone concentrations reported for adult males (male high testosterone); pink: model output distribution for simulations incorporating sex hormone concentrations of adult females at menses at the time of injury (female low estradiol, low progesterone); black: model output distribution for simulations incorporating sex hormone concentrations of adult females at the peri-ovulatory phase of the menstrual cycle (female peak estradiol, low progesterone) at the time of injury. For IL-1 β , there are significant differences between every possible hormone pair: “male” is significantly different from “female peri-ovulation”; “male” is significantly different from “female menses”; and “female peri-ovulation” is significantly different from “female Menses.” IL-10 is significantly different between “male” and “female peri-ovulation” through $t = 11$ days and $t = 2$ days between “female peri-ovulation” and “female menses.” MMP-3 was significantly different between “male” and “female peri-ovulation” at $t = 1$ day. TNF- α shows no significant differences between “female menses” and “female peri-ovulation” at any time point. These observed endocrine effects on IL-1 β , IL-10 and TNF- α are consistent with our findings from our previous model³². Further, no differences exist between hormone conditions at $t = 0$ days, since the initial conditions are the same regardless of the hormone treatment. Figure created using GraphPad Prism version 10.2.2 for Windows, GraphPad Software, Boston, Massachusetts USA, <https://www.graphpad.com>^{39,41–48}.

female menses condition, male simulations showed significantly reduced IL-1 β [simulation day 1–16, $p < 0.001$]. In female peri-ovulatory simulations, IL-1 β [simulation day 1–12, $p < 0.001$] and MMP-3 [simulation day 1, $p < 0.001$] increased significantly, while IL-10 decreased [simulation day 1–2, $p < 0.001$] compared to female menses. Notably, from simulation days 14–16, IL-1 β distributions under the female peri-ovulation condition were significantly suppressed [$p < 0.001$] compared to female menses. TNF- α post-injury distributions were also considerably lower in male simulations compared to female peri-ovulation and menses throughout the analysis duration [$p < 0.001$]. However, TNF- α distributions did not significantly differ between female peri-ovulation and menses conditions at any time point.

An example of disparities in model output distributions between male and female endocrine states for IL-1 β , TNF- α , and MMP-3 can be seen at simulation day 1. Male simulations demonstrated significantly lower levels of IL-1 β [8.70 (10.48–7.19) pg/mL] and TNF- α [2.12 (3.42–1.29) pg/mL] compared to female peri-ovulation [IL-1 β : 17.34 (21.15–14.26) pg/mL, $p < 0.001$; TNF- α : 10.13 (12.13–8.35) pg/mL, $p < 0.001$] and menses simulations [IL-1 β : 10.46 (12.48–8.60), $p < 0.001$; TNF- α : 10.41 (12.33–8.71) pg/mL, $p < 0.001$]. MMP-3 output distributions were significantly lower in male simulations [MMP-3: 249.00 (282.34–217.19) ng/mL] compared to female peri-ovulation simulations [MMP-3: 275.80 (315.98–241.61) ng/mL, $p = 0.001$]. Conversely, IL-10 output distributions were significantly higher in male simulations [31.47 (37.71–26.99) pg/mL] compared to female peri-ovulatory simulations [24.34 (28.82–20.53) pg/mL, $p < 0.001$].

The output distributions for IL-6, TGF- β , MMP-1, MMP-9, MMP-13, and TIMP-1 did not exhibit significant differences between the female and male endocrine conditions at any simulated time point.

Discussion

Despite extensive efforts, translating basic science research findings into effective treatments for post-traumatic joint inflammation and cartilage destruction in humans has proven challenging. One reason for this difficulty is the failure to account for the complex, nonlinear nature of the acute inflammatory process after injury and the influence of external factors such as sex and endocrinological state. While in silico modeling has shown promise in helping researchers understand inflammation mechanisms, only two models have been developed to investigate inflammation in the human synovial joint, one of which was developed by our group^{33,34}. The findings from our model in this study corroborate both established hypotheses: elevated estradiol levels in simulations during the female peri-ovulatory phase promote pro-inflammatory effects by increasing IL-1 β expression and decreasing IL-10 expression post-trauma. In contrast, male hormone levels exhibit anti-inflammatory effects on

simulations by reducing IL-1 β , TNF- α , and MMP-3 expression following trauma compared to pre-menopausal females. These findings support our earlier *in silico* findings³⁴ as well as various clinical observations that menstrual hormone variations in young females can influence acute inflammatory and catabolic processes after joint trauma, potentially contributing to poorer outcomes compared to males^{49,50}.

In the absence of hormones, our *in-silico* model effectively captured key kinetic aspects of the local inflammatory and catabolic response in the synovial environment following trauma, as supported by direct comparisons with available *in vivo* experimental data. Using Sobol sensitivity analysis, we demonstrated that the simulated outputs for cytokines IL-1 β , TNF- α , IL-6, and IL-10 post-injury are primarily influenced by parameters associated with the rate of macrophage influx and efflux in the synovium, as well as the rate of macrophage production of cytokines. These factors contribute to over 50% of the total output variance for these molecules throughout the simulation duration. The increased output of chemokine factors like TGF- β and TNF- α in the SF after injury primarily triggers macrophage influx into the synovial cavity post-injury⁵¹⁻⁵³. Upon entering the synovial cavity, macrophages adopt a pro-inflammatory phenotype (M1), triggering inflammatory mechanisms linked to pathological cartilage resorption in resident joint cells. This occurs through the secretion of pro-inflammatory cytokines, disrupting synovial tissue homeostasis⁵⁴. It remains to be examined to what extent the significant contribution of macrophage chemotaxis affects the regulation of acute joint inflammation, contingent upon the model assumptions. It is important, however, to recognize that inflammatory cytokines in the post-injury synovial joint are not solely produced by invading macrophages. Both chondrocytes⁵⁵ and synovial fibroblasts⁵⁶ contribute to acute inflammation and subsequent tissue remodeling following injury, as confirmed by our Sobol analysis on the cytokine model outputs. Although their impact on cytokine production ranked lower than macrophages in this model, future research should account for these resident cells and their interactions with invading macrophages when investigating the joint's biological environment post-injury.

While macrophages constitute the most abundant immune cells in the synovium, ranging from 12 to 40% of synovial immune cells^{57,58}, recent human *in vivo* evidence highlights the importance of T-cell infiltration into the synovial fluid following joint trauma⁵⁹. CD4+ T-cells, commonly known as T helper cells, are notably abundant among T-cell infiltrates in injured joints compared to healthy joints⁵⁹. However, the heterogeneity of T-cell subtypes⁶⁰ and the time-course profile of T-cell infiltrates⁵⁹ in human injured joints still need to be better understood, presenting challenges in quantifying T-cell kinetics within the current model. Specifically, Kim-Wang et al. 2021⁵⁹ reported the first quantifiable data on T-cell subpopulation infiltration into a non-arthritis post-injury joint; however, this study did not report post-injury T-cell kinetic data. In the inflamed synovium of rheumatoid arthritis patients, T-cells adjacent to macrophages have been shown to prompt cytokine production⁶¹, either through direct cell interactions⁶² or by releasing cytokines like IL-17, which are known to stimulate catabolic processes in chondrocytes and synovial fibroblasts⁶³. These observations suggest that post-injury synovial T-cell infiltration may occur downstream of increases in monocytes and macrophages. Incorporating time-course data on CD-4+ kinetics into the current framework would significantly enhance the comprehensiveness of the acute post-injury immune response and offer opportunities for investigating immune cell pathways associated with PTOA onset, potentially leading to the development of targeted therapeutic interventions.

After verifying the plausibility of the model output concentrations with *in vivo* SF data from healthy and non-injured human knee joints, we utilized hormonal profiles from blood serum data collected from 22 young, healthy female subjects to explore the impact of fluctuating sex hormone concentrations throughout the menstrual cycle. Comparing LHS model simulations initiated on each day of the menstrual cycle, we found that elevated concentrations of estradiol during the peri-ovulatory (cycle day 15) led to an overexpression of the pro-inflammatory cytokine IL-1 β and suppression of the anti-inflammatory cytokine IL-10 post-injury. Prior epidemiological studies have suggested links between menstrual hormone fluctuations and joint injury risk, particularly during peri-ovulation⁶⁴. Estradiol has been shown experimentally to have concentration-dependent effects on inflammatory mechanisms⁶⁵; however, the impact of these effects on the *in vivo* synovial post-injury response in female humans is unclear⁶⁶. Our findings highlight the potential of this computational framework in guiding future research to explore the effects of estradiol fluctuations on cellular remodeling processes influenced by inflammatory molecules like IL-1 β and IL-10⁶⁷. By complementing *in vitro* experiments with *in silico* modeling, researchers can enhance experimental design efficiency and gain deeper insights into sex-specific endocrine dynamics affecting complex biological systems such as the synovial joint.

Our analysis, focusing on the influence of sex-specific hormone profiles, revealed notable findings concerning the impact of testosterone, a predominantly male hormone, on post-injury inflammation and catabolism within the joint. Simulations incorporating male concentrations of testosterone demonstrated decreased post-injury outputs of IL-1 β , TNF- α , and MMP-3, along with elevated levels of IL-10 compared to the female endocrine conditions. Our model findings are corroborated by previous experimental investigations that reported reductions in IL-1 β , TNF- α , and MMP-3 expression, alongside increases in IL-10 expression following testosterone incubation^{68,69}. The suppression of inflammatory cytokines and synovial fluid MMP-3 activity, initiated by testosterone signaling, may potentially improve post-injury outcomes in males relative to females. This is particularly significant given that MMP-3 activates latent forms of MMP-1⁷⁰ and MMP-9⁷¹ to cartilage matrix degradation. The current model framework provides insights into the dimorphic impacts of male and female sex hormones on acute joint inflammation and cartilage degradation mechanisms, highlighting the therapeutic potential of targeting hormone-related pathways, such as testosterone, to manage post-injury outcomes in both genders⁷².

Limitations

One primary limitation of this study arises from the necessary simplifications to develop a mathematical representation of the intricate cellular and molecular interactions within the joint microenvironment. The

present model focuses on a subset of cytokines, chemokines, and growth factors that influence MMP expression following joint trauma. The inclusion of substances in this study was partly determined by the limited availability of in vivo datasets in human synovial fluid (SF) necessary to verify the model outputs, such as continuous time-course biomarker data collected within a month post-injury^{37,38,40,73}. Since the primary objective of this model is to investigate protein kinetics within the joint and the sex-specific factors influencing these kinetics during the acute phase of injury, the inclusion of in vivo studies that report biomarker data within the early to late sub-acute period post-injury (1–30 days)⁷⁴ while also accounting for patient sex or endocrinological state are essential. Such data sets would be needed to conduct quantitative statistical assessment to the model projections to verify the present construct and support the inclusion of additional substances in future model iterations.

Moreover, substance inclusion was also impacted by the availability of in vitro datasets needed for model parameterization. For example, insulin-like growth factor (IGF)-1, a growth factor known for its importance in the synovial catabolic/anabolic axis⁷⁵, was omitted due to limited literature reporting in vitro protein kinetic data in joint cell units necessary for the parameterization of production, clearance, and feedback inputs to construct the equations in this model. This limitation, shared by other excluded molecules and metabolites⁷⁶, underscores the need for additional experimental studies investigating joint cell protein kinetics to support their inclusion.

While verifying the plausibility of our model substance initial conditions, we found notable differences between the outputs for TGF- β , MMP-9, and MMP-13 and reported experimental measurements in healthy human synovial fluid. These discrepancies may arise from two potential factors: either our model insufficiently accounted for accurate concentrations of resident cellular constituents within the healthy synovium, or uncertainties exist in the experimental measurements conducted in human in vivo studies. In our study, we assumed that resident joint cellular concentrations in our simulations would correspond to widely used in vitro cell density values due to limited data availability on specific cellular concentrations within the human synovium⁷⁷. Furthermore, limitations in human in vivo studies, including small sample sizes⁷⁸, and experimental uncertainties such as undetected sub-acute joint inflammation or uncontrolled variables^{79,80}, may also contribute to discrepancies between experimental concentrations and model predictions. In the context of our predictions for TGF- β , human in vivo studies have reported low or absent TGF- β values in healthy joint SF⁴¹. For example, Fang et al.⁸¹ reported that the lower detection threshold of the assay used to measure TGF- β was 7 pg/ml, which encompasses our healthy model prediction. Thus, the initial healthy value for TGF- β in our study is plausible given the literature. However, future clinical research is needed to validate these initial conditions by measuring the concentrations of TGF- β in synovial fluid aspirated from human knee joints at a resting baseline using a more sensitivity assay⁸². Furthermore, our healthy model prediction for MMP-9 is primarily influenced by the presence of macrophages in the system. In our model, assuming that at the initial state the joint is healthy, we assume that macrophages are not active in the environment⁸³. Consequently, our model may inaccurately estimate MMP-9 concentration without the contribution of inactive synovial macrophages. However, prior limited literature sources suggest variability in MMP-9 levels in healthy human knee SF. For example, in 12 subjects, Iverson et al.⁸⁴ reported SF MMP-9 levels at 122.50 (4300.56) pg/mL in non-injured contralateral knees, supporting the plausibility of our initial concentration prediction in this model.

To investigate the effect of sex hormones on post-injury inflammation and tissue remodeling in the synovium, we integrated seven hormonal feedback functions into our model. However, only the feedback parameters for the present hormones were solely included for macrophages. While the presence of hormone receptors in resident joint cells is recognized^{26,85}, limited in vitro studies have explored sex hormone effects on the basal cellular production of the substances in our model. Additionally, sex hormones influence intracellular signaling pathways related to molecule interactions, like cytokine induced MMP production⁸⁶. However, experimental data for incorporating these feedback effects into our model is also lacking. Therefore, our model likely incompletely captures the comprehensive impact of sex hormone feedback on joint metabolism post-injury. Further experimental investigations are needed to understand the specific effects of hormones on cellular inflammatory metabolism, which can contribute to refining our model and enhancing prediction accuracy.

Additionally, this study solely focuses on the hormonal effects associated with pre-menopausal females. Several factors drove the decision to narrow the scope to this demographic. Firstly, epidemiological evidence indicates that peri- and post-menopausal females face an increased risk of osteoarthritis, potentially linked to variations or deficiencies in the endogenous hormone cycle^{13,87}. Although the underlying biological mechanisms impacted by hormonal deficiencies in musculoskeletal tissue remain enigmatic, one can imagine incorporating independent hormonal states that represent peri- or post-menopausal females⁸⁸. Furthermore, exploring hormone effects in an aging population introduces additional sources of covariance, such as the impact of cellular senescence⁸⁹ and altered synovial metabolism resulting from preexisting tissue wear⁶⁸. These confounders likely influence the inflammatory and remodeling response under investigation. To address these sources of variability within our current framework, sex hormone data must be collected from peri- and post-menopausal women to establish hormonal profiles for each endocrine condition in this construct³⁶; model parameters need to be developed to incorporate the effects of senescence on cellular molecule production. Ultimately, there is a lack of quantitative understanding of the effects of sex hormone deficiency⁹⁰ and aging on joint cell metabolism⁸⁹ hindering a comprehensive model-based synthesis of these states.

Conclusion

Through our quantitative framework, our primary objective was to elucidate specific mechanisms responsible for increased inflammation and cartilage damage in the joint post-trauma while considering the influence of sex and endocrinological factors. Our model simulations revealed that elevated estradiol levels in pre-menopausal females increased the expression of pro-inflammatory cytokine IL-1 β and inhibited the expression of anti-inflammatory cytokine IL-10 after simulated injury. Furthermore, heightened testosterone levels in males decreased the simulated expression of IL-1 β , TNF- α , and MMP-3 while increasing IL-10 production compared

to female endocrine states. The culmination of these model findings establishes a robust quantitative basis for exploring the intricate interplay of biology and sex endocrinology in post-injury inflammation and catabolism within the joint. This mathematical framework can inform the design of future clinical and experimental studies aimed at replicating the present findings, thus advancing our understanding of the cellular mechanisms underlying the onset of PTOA and the impact of sex and endocrinological factors on joint health. Furthermore, this modeling approach has the potential to aid in the development of patient-specific pharmaceutical interventions targeting the reduction of inflammation and matrix metalloproteinase activity in the injured joint while considering the individual's biological and endocrine state.

Methods

Model equations

Our mathematical model represents the metabolic response within the synovial joint after traumatic injury (see Fig. 7A). A system of first-order differential equations was used to model the post-injury interaction by resident populations of chondrocytes and synovial fibroblasts along with migrating macrophages in MATLAB R2019b Software (The MathWorks Inc, MA, USA). Twelve molecular substances were targeted in the present computational framework (please see Table 1). The network of interactions between the cells and molecular substances within the trauma model is shown in Fig. 7B. It is based on molecular kinetics data reported in vitro in over 60 usable publications from the PubMed database. A generalized form of the twelve model equations in this construct is summarized in Eq. 1.^{32,34}:

$$\frac{dC_x}{dt} = \left(\prod_m g_{m,x} \right) k_{x,M1} C_{M1} + k_{x,M2} C_{M2} + \left(\prod_s g_{s,x} \right) k_{x,SF} C_{SF} + \left(\prod_c g_{c,x} \right) k_{x,CH} C_{CH} - k_{d,x} C_x \quad (1)$$

where C_x is the concentration of a molecular substance x , $k_{x,M1}$ is the baseline production rate of substance x by M_1 macrophages, $k_{x,M2}$ is the production rate of substance x by M_2 macrophages, $k_{x,SF}$ is the baseline production rate of substance x by SFs, $k_{x,CH}$ is the production rate of substance x by chondrocytes, C_{M1} is the concentration of M_1 macrophages, C_{M2} is the concentration of M_2 macrophages, C_{SF} is the concentration of SFs, C_{CH} is the concentration of chondrocytes, $k_{d,x}$ is the degradation rate for substance x , $g_{m,x}$ describes the feedback regulation of substance x by substance m in M_1 macrophages, $g_{s,x}$ describes the feedback regulation of substance x by

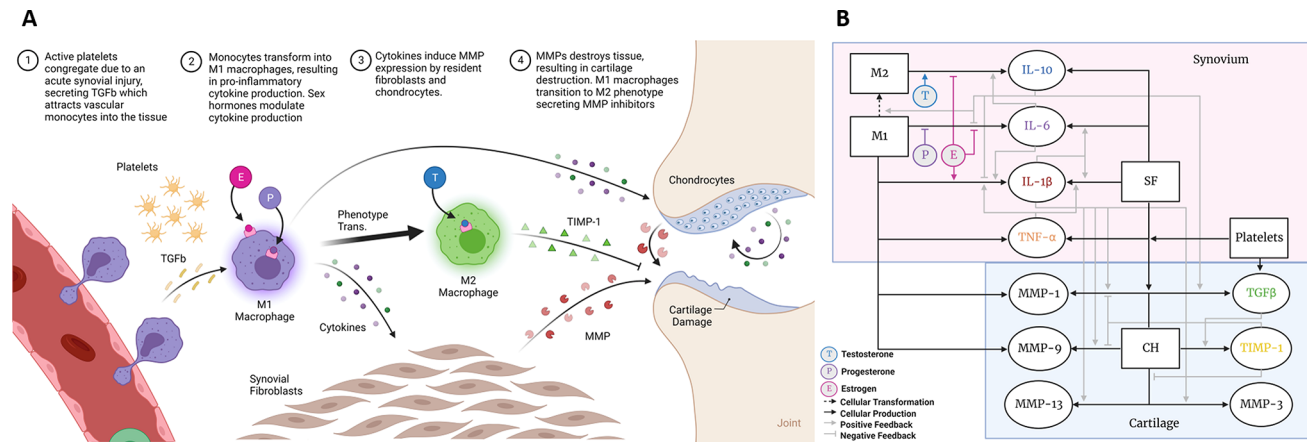


Fig. 7. (A) Graphic depiction of the trauma associated inflammatory cascade in the synovium. Knee joint injury triggers the release of chemoattractants, including TNF- α and TGF- β , which stimulate the migration of monocytes from the bloodstream to the synovium, depicted by the red shading. These monocytes undergo a transformation into pro-inflammatory M1 macrophages⁹¹. The M1 macrophages then produce inflammatory mediators that interact with resident synovial fibroblasts and chondrocytes, resulting in the release of additional cytokines and MMPs. The anti-inflammatory process is initiated by IL-10, which drives the conversion of M1 cells into anti-inflammatory M2 macrophages. (B) Cellular production and feedback regulation of substances incorporated in the model. This schematic shows the physiological process modeled in this study using a subset of the incorporated production and feedback parameters. M1, M2, SF and CH produce IL-10^{92–94}, IL-1 β ^{92,93}, TNF- α ^{92,93,95}, IL-6^{96,97}, and TIMP-1^{98,99}. MMP-1 is produced by SF¹⁰⁰, and CH¹⁰¹. MMP-9 is produced by M1 and M2.¹⁰² MMP-3 and MMP-13 are produced by CH^{103,104} and SF^{99,105}. IL-10 down-regulates M1 production of IL-1 β and IL-6¹⁰⁶, while IL-1 β up-regulates SF production of IL-1 β ¹⁰⁶, IL-6⁹⁷, and MMP-9⁹⁹ and CH production of MMP-1¹⁰⁷, MMP-3¹⁰⁷, and MMP-13¹⁰⁸. IL-6 up-regulates M1 IL-10¹⁰⁹ and IL-1 β ¹¹⁰. TNF- α upregulates SF and CH IL-1 β ^{24,111}. Estrogen (E) up-regulates M1 production of IL-1 β ¹¹² and down-regulates M1 production of IL-10¹¹³ and IL-6¹¹⁴, while testosterone (T) up-regulates M1 production of IL-10¹¹³. Progesterone (P) down-regulates M1 IL-6¹¹⁵. A full summary of all model production and feedback inputs as well as supporting data can be found Tables S3 and S4. M1: pro-inflammatory macrophage. M2: anti- inflammatory macrophage. SF: synovial fibroblast. CH: chondrocyte. Figure created with BioRender.com.

substance s in SFs, $g_{c,x}$ describes the feedback regulation of substance x by substance c in chondrocytes, and Π is the product operator.

Molecular kinetic parameters

Our approach for formulating the kinetic parameters for each of the molecular substances in our model is reliant on two sets of in vitro data: (1) input parameters defining the kinetics of cellular constituencies under basal and endocrine-specific conditions and (2) the feedback functions that drive the post-trauma metabolic cascade. Input parameters defining the cellular production ($k_{x,y}$) and clearance for all modeled substances under basal conditions ($k_{d,x}$) were identified from previous in vitro examinations and calculated using the functions outlined in our prior model³⁴ which is like the formulation reported by Nagaraja et al.³² also describe the procedure of calculating the production and clearance inputs in S1 Text for completeness. A summary of the computed production and clearance input values used in the present model can be found in Table S3. In total, we included 49 production and decay coefficients in our model, which we derived from 32 published reports.

We used monotonically increasing and decreasing feedback functions ($g_{j,x}$) to describe the positive and negative changes in the production of a given molecular substance by other molecules in the synovium based on numerous cellular-level in vitro experiments. Table S4 lists all the estimated parameters for the positive and negative feedback functions. For clarity, we also included a detailed description of the process for formulating the positive and negative feedback functions used in this model in the S1 Text. In total, we included 58 feedback functions in our present model, which we derived from 32 published reports. These reports were selected through an in-depth literature review conducted using the PubMed database, utilizing both the "Best Match" and "Most Recent" features. For each substance, we employed relevant keywords such as "MMP-1 IL-1 β treated chondrocytes" and "in vitro MMP-1 concentration IL-1 β treated chondrocytes," replacing "MMP-1" and "IL-1 β " with the names of any paired biomarker feedback under consideration and "chondrocytes" with the target cell type.

Although protein kinetics associated with human immune cells under endocrine treatment conditions are widely reported, kinetic parameters associated with sex hormone treatment of human resident synovial cells (synovial fibroblasts and chondrocytes) are lacking. Thus, in this present model, endocrine feedback parameters were not included for chondrocytes and synovial fibroblasts.

Cellular kinetic parameters

Our formulation of cellular kinetic parameters for synovial fibroblasts, chondrocytes, and macrophages closely follows the established methodology outlined in our prior work³⁴. It is essential to highlight that the exact cellular concentrations of synovial fibroblasts and chondrocytes in healthy SF still need to be defined. Consequently, for our simulations, we adopted widely used in vitro cellular concentrations ($5 * 10^5$ cells/ml) for both cell types as initial conditions⁷⁷. We assumed a constant concentration for synovial fibroblasts and chondrocytes throughout each simulation while allowing for variable macrophage concentrations within the synovium. To prompt macrophage migration into the injured synovial environment, we harnessed signals from TGF- β and TNF- α produced by platelets. To simulate trauma-induced macrophage migration, we integrated chemotactic functions ($f_{TGF,M1}, f_{TNF,M1}$) into the current model. For specific parameter values, please refer to Table S4.

To initiate the injury-induced inflammatory response within our model, we established the initial platelet concentration at $2 * 10^8$ platelets/ml³². Additionally, in alignment with previous computational investigations into injury-induced inflammation^{32,34}, we implemented a condition where the macrophage chemotactic functions were maintained at zero when platelet concentrations dropped below a predetermined threshold level ($10 * 10^{-12}$ platelets/mL). This precautionary measure was undertaken to prevent any non-physiological re-initiation of inflammation. Although this threshold concentration lacks physiological grounding, it serves a practical computational purpose and has been effectively employed in previous models^{32,34} to avert unintended outcomes.

Determination of initial conditions

To characterize the cellular environment of a healthy synovial joint before any injury occurred, we conducted preliminary simulations with chondrocytes and synovial fibroblasts as the sole producers of proteins, excluding immune cellular constituents. This simulation was run for 1.25 h (using a single CPU core on a custom workstation equipped with an AMD Ryzen 9 3900X processor and 32 GB of RAM), and the results allowed us to approximate the initial steady-state concentrations for each molecule. Subsequently, these steady-state concentrations served as the initial conditions for all simulations involving immune cells, following a technique described previously³⁴. A summary of the initial conditions for each modeled substance can be found in Table 1.

Determination of female and male sex hormone profiles

We implemented a nonlinear mixed effect model (NLME) with harmonic terms to generate comprehensive profiles for the sex hormones estradiol, progesterone, and testosterone throughout the human female menstrual cycle. The harmonic model employed in this construct is based on a previous model developed by Mumford et al.³⁶ In Fig. 2, we present a collective representation of reported systemic estradiol, progesterone, and testosterone profiles during the female menstrual cycle. These profiles were created by using a normalizing ensemble of the NLME model fit of serum hormone data collected from 22 healthy female subjects in a previous study completed by our group²⁹. All participants provided written informed consent. This study was approved by the University of Texas Southwestern Medical Center Institutional Review Board and was conducted in accordance with the Helsinki Declaration.

To generate the group representative profile for each hormone in females, we calculated the mean and standard deviation of the fitted hormone concentrations using the MATLAB R2022a Statistics and Machine

Learning Toolbox. These representative profiles were then incorporated into our mathematical modeling process, providing a robust and comprehensive representation of sex hormone dynamics and variability throughout the human female menstrual cycle.

In addition to the female hormonal conditions, we also incorporated a static male hormonal condition that accounts for concentration of serum sex hormones reported in male humans *in vivo*^{116,117}.

Uncertainty modeling and analysis

To ensure the robustness of our model and account for potential uncertainty in the biologically derived input parameters, we employed Latin Hypercube Sampling (LHS), a statistical sensitivity analysis method commonly used in computer simulation applications¹¹⁸. Utilizing the MATLAB function LHSDESIGN, we introduced random variations to each calculated production and clearance coefficient within a range of $\pm 60\%$ of its nominal value, resulting in the generation of 1,000 unique input parameter sets. These randomized sets of inputs produced corresponding outputs of the differential equations, providing a comprehensive evaluation of the model's behavior under varied conditions. The selection of the LHS sampling range was based on the variability of the in vitro data used to formulate the input parameters. Citations linked to the reported data can be found in Table S3. This simulation was run for 1.81 h (using a single CPU core on a custom workstation equipped with an AMD Ryzen 9 3900X processor and 32 GB of RAM).

We determined the median and interquartile range values for each substance's output at every simulated time point to generate likelihood estimates for our modeled results that accounted for experimental uncertainties associated with the input parameters. These likelihood estimates were generated without hormones to enable fair comparisons with independent *in vivo* data that did not account for hormonal effects.

Verification of model predictions

To investigate the acute molecular kinetics in the synovial joint after traumatic injury, we conducted an extensive literature review by searching the PubMed database, utilizing the "Best Match" and "Most Recent" features. For each substance, we employed relevant keywords such as "MMP concentration synovial fluid" and "in vivo MMP synovial concentration," replacing "MMP" with the name of any individual biomarker under consideration. Additionally, we combined these terms with "Knee Injury" and "healthy" to gather studies focusing on healthy synovial fluid biomarker concentration in the states simulated within our model.

Global sensitivity analysis

Traditional sensitivity analysis techniques, often assuming model linearity, focus on varying individual input parameters in isolation. These local sensitivity analysis (LSA) methods aim to assess model behavior at specific points¹¹⁹. However, complex *in silico* constructs, like the present model, are generally nonlinear and involve interactions among multiple parameters. As a result, global sensitivity analysis (GSA) methods offer a more suitable approach. In contrast to LSA methods, GSA techniques simultaneously vary all input variables across their entire sample ranges. The sensitivity index, quantifying the relative importance of each input factor, measures the fractional contribution to the output variance. Among various existing methods, the Sobol Method¹²⁰ is one of the most established and widely used techniques in computational biology. This method computes the first order and total-order sensitivity indices, capturing both the main effects of a given input parameter and all interactions (of any order) within the model system involving that parameter³⁰.

In our current work, we adopted GSA techniques using the SAFE (Sensitivity Analysis For Everybody) toolbox¹²¹ to assess the impact of the top 5 ranked input parameters on the output variance for each of the modeled substances in the absence of hormonal effects over 100,000 simulated iterations. This simulation was run for 144 h (using a single CPU core on a custom workstation equipped with an AMD Ryzen 9 3900X processor and 32 GB of RAM). Detailed implementation of this GSA method has been previously described in other studies¹²². Figure 1 schematically depicts the modeling process used in the present study. It is worth noting that inclusion of other molecules of interest will significantly increase computational time; hence, the use of high-powered computing (HPC) systems is recommended.

Female and male hormone analysis

We conducted two analyses to explore the effects of sex hormones on the post-injury response of inflammatory and catabolic molecules in the joint. Firstly, we performed simulations using the combined female menstrual hormone profiles of estrogen, progesterone, and testosterone. Our objective was to investigate how hormone concentrations at key points in the menstrual cycle influence the dynamics of the modeling results. To achieve this, we employed LHS to vary the model coefficients and the mean concentrations of the NLME-fitted sex hormones by $\pm 20\%$. Subsequently, we initialized the present mathematical model at each day of the menstrual cycle (cycle day 1–30), comparing the model outputs over time. Throughout these simulations, we also assessed the maximum projected concentrations for each molecular substance to determine whether changes in the menstrual endocrine state impacted the overall severity of the acute response post-injury.

Having examined the effects of fluctuating hormone concentrations during the female menstrual cycle, we proceeded to conduct a second set of simulations to investigate the influence of male sex hormone concentrations on the model outputs. Our objective in this analysis was to explore the potential existence of sex dimorphism in the inflammatory and catabolic response. For this purpose, we incorporated the male endocrine condition into the model, comprising of high static concentrations of testosterone and low static concentrations of estrogen and progesterone. The outputs of this simulation in males would be compared to the female endocrine conditions at menses and peri-ovulation.

Statistical analysis

To evaluate the influence of female menstrual hormone fluctuations (estradiol, progesterone, and testosterone) on the distribution of maximum output values for each modeled substance, we employed rank-based covariate (RBC) adjustment methods¹²³. These methods allow comparison of model outputs from different groups while accommodating non-normality in the covariate and output data. Both model output distributions and covariates were found to be non-normal and were transformed into ranks. Hormone covariance was adjusted using linear regression of ranked model output data with ranked hormone covariates. An analysis of variance with Dunn's multiple comparisons test was conducted on the equality of residual values among groups obtained from the linear regression of ranked maximum outputs to ranked covariates from injury simulations initiated at various menstrual phases: menses (cycle day 0), mid-follicular (cycle day 7), peri-ovulatory (cycle day 15), early luteal (cycle day 18), and late luteal (cycle day 26). Statistical significance for these comparisons was adjusted using Šidák correction, reducing the threshold from 0.05 to 0.0051.

To assess the influence of sex-specific endocrine states on modeled substance outputs, we employed RBC methods to compare differences in output distributions among the "Female Peri-Ovulation," "Female Menses," and "Male" model conditions at each simulated day, up to $t = 30$ days. Statistical significance for these comparisons was adjusted using Šidák correction, lowering the threshold from 0.05 to 0.017. RBC analysis and Dunn's post hoc test for all comparisons in this study were performed using MATLAB R2022a software with Cardillo G.'s (2006) Dunn's Test procedure for multiple, non-parametric comparisons (<http://www.mathworks.com/matlabcentral/fileexchange/12827>).

Data availability

All required cell and molecule data sets for the current study are reported in supplemental Tables 3 and 4. The female subject endocrine data is included in the model code file. All model results generated during the current study are freely available on GitHub. (<https://github.com/ConnerHutcherson/In-Silico-Knee-Trauma-Model>).

Code availability

The MATLAB scripts used for our computational analyses are freely available on GitHub (<https://github.com/ConnerHutcherson/In-Silico-Knee-Trauma-Model>).

Received: 2 September 2024; Accepted: 24 October 2024

Published online: 19 November 2024

References

- Thomas, A. C., Hubbard-Turner, T., Wikstrom, E. A. & Palmieri-Smith, R. M. Epidemiology of posttraumatic osteoarthritis. *J. Athl. Train.* **52**, 491–496 (2017).
- Samuels, J., Krasnokutsky, S. & Abramson, S. B. Osteoarthritis: A tale of three tissues. *Bull. NYU Hosp. Jt. Dis.* **66**, 244–250 (2008).
- Ingram, J. G., Fields, S. K., Yard, E. E. & Comstock, R. D. Epidemiology of knee injuries among boys and girls in US high school athletics. *Am. J. Sports Med.* **36**, 1116–1122 (2008).
- Prodromos, C. C., Han, Y., Rogowski, J., Joyce, B. & Shi, K. A meta-analysis of the incidence of anterior cruciate ligament tears as a function of gender, sport, and a knee injury-reduction regimen. *Arthrosc. J. Arthrosc. Relat. Surg.* **23**, 1320–1325 (2007).
- Hollis, B. et al. Lifetime risk and genetic predisposition to post-traumatic OA of the knee in the UK Biobank. *Osteoarthr. Cartil.* **31**, 1377–1387 (2023).
- Blaker, C. L., Ashton, D. M., Doran, N., Little, C. B. & Clarke, E. C. Sex-and injury-based differences in knee biomechanics in mouse models of post-traumatic osteoarthritis. <https://doi.org/10.17632/z754455x3c1>.
- Welhaven, H. D. et al. Metabolic phenotypes reflect patient sex and injury status: A cross-sectional analysis of human synovial fluid. *Osteoarthr. Cartil.* <https://doi.org/10.1016/j.joca.2023.09.004> (2023).
- Sinclair, J. & Selfe, J. Sex differences in knee loading in recreational runners. *J. Biomech.* **48**, 2171–2175 (2015).
- Park, S.-K., Stefanyshyn, D. J., Loitz-Ramage, B., Hart, D. A. & Ronsky, J. L. Changing hormone levels during the menstrual cycle affect knee laxity and stiffness in healthy female subjects. *Am. J. Sports Med.* **37**, 588–598 (2009).
- Gokhale, J. A., Frenkel, S. R. & Dicesare, P. E. Estrogen and osteoarthritis. *Am. J. Orthop. (Belle Mead NJ)* **33**, 71–80 (2004).
- Tankó, L. B., Søndergaard, B.-C.C., Oestergaard, S., Karsdal, M. A. & Christiansen, C. An update review of cellular mechanisms conferring the indirect and direct effects of estrogen on articular cartilage. *Climacteric* **11**, 4–16 (2008).
- Sniekers, Y. H., Weinan, H., Bierma-Zeinstra, S. M., van Leeuwen, J. P. T. M. & van Osch, G. J. V. M. Animal models for osteoarthritis: The effect of ovariectomy and estrogen treatment—A systematic approach. *Osteoarthr. Cartil.* **16**, 533–541 (2008).
- Watt, F. E. Hand osteoarthritis, menopause and menopausal hormone therapy. *Maturitas* **83**, 13–18 (2016).
- Sandell, L. & Aigner, T. Articular cartilage and changes in arthritis An introduction: Cell biology of osteoarthritis. *Arthritis. Res.* **3**, 337–341 (2001).
- Burrage, P. S., Mix, K. S. & Brinckerhoff, C. E. Matrix metalloproteinases: Role in arthritis. *Front. Biosci.* **11**, 529–543 (2006).
- Mehana, E. S. E., Khafaga, A. F. & El-Blehi, S. S. The role of matrix metalloproteinases in osteoarthritis pathogenesis: An updated review. *Life Sci.* **234**, 116786 (2019).
- D'agostino, P. et al. Sex hormones modulate inflammatory mediators produced by Macrophages. *Ann. N. Y. Acad. Sci.* **876**, 426–429 (1999).
- Xue, X. T. et al. Progesterone attenuates temporomandibular joint inflammation through inhibition of NF-κB pathway in ovariectomized rats. *Sci. Rep.* **7**, 1–8 (2017).
- Straub, R. H. The complex role of estrogens in inflammation. *Endocr. Rev.* **28**, 521–574 (2007).
- Hunt, J. S., Miller, L. & Platt, J. S. Hormonal regulation of uterine macrophages. *Dev. Immunol.* **6**, 105–110 (1998).
- Ralston, S. H., Russell, R. G. & Gowen, M. Estrogen inhibits release of tumor necrosis factor from peripheral blood mononuclear cells in postmenopausal women. *J. Bone Miner. Res.* **5**, 983–988 (1990).
- Asai, K. et al. Gender differences in cytokine secretion by human peripheral blood mononuclear cells: Role of estrogen in modulating LPS-induced cytokine secretion in an ex vivo septic model. *Shock* **16**, 340–343 (2001).
- Lu, T., Achari, Y., Sciore, P. & Hart, D. A. Estrogen receptor alpha regulates matrix metalloproteinase-13 promoter activity primarily through the AP-1 transcriptional regulatory site. *Biochim. Biophys. Acta Mol. Basis Dis.* **1762**, 719–731 (2006).
- Ganesan, K., Balachandran, C., Manohar, B. M. & Puvanakrishnan, R. Effects of testosterone, estrogen and progesterone on TNF-α mediated cellular damage in rat arthritic synovial fibroblasts. *Rheumatol. Int.* **32**, 3181–3188 (2012).

25. Claassen, H. et al. 17 β -estradiol reduces expression of MMP-1, -3, and -13 in human primary articular chondrocytes from female patients cultured in a three dimensional alginate system. *Cell Tissue Res.* **342**, 283–293 (2010).
26. Kinney, R. C., Schwartz, Z., Week, K., Lotz, M. K. & Boyan, B. D. Human articular chondrocytes exhibit sexual dimorphism in their responses to 17 β -estradiol. *Osteoarthr. Cartil.* **13**, 330–337 (2005).
27. Polan, M. L., Daniele, A. A. & Kuo, B. A. FERTILITY AND STERILITY Gonadal Steroids Modulate Human Monocyte Interleukin-1 (IL-1) Activity* Monocyte Isolation and Culture With Heparinized Tubes, Blood Was Collected from Healthy Male Volunteers with No History of Recent Fertility and Sterility, vol. 49 (1988).
28. Rovensky, J. et al. Gonadal and adrenal steroid hormones in plasma and synovial fluid of patients with rheumatoid arthritis. *Endocr. Regul.* **38**, 143–149 (2004).
29. Soedirdjo, S. D. H., Rodriguez, L. A., Chung, Y. C., Casey, E. & Dhaher, Y. Y. Sex hormone-mediated change on muscle activation deactivation dynamics in young eumenorrheic women. *Front. Physiol.* **14**, 1–10 (2023).
30. Sobol, I. M. Sensitivity estimates for nonlinear mathematical models. In (1993).
31. Geris, L., Schugart, R. & Van Oosterwyck, H. In silico design of treatment strategies in wound healing and bone fracture healing. *Philos. Trans. R. Soc. A Math. Phys. Eng. Sci.* **368**, 2683–2706 (2010).
32. Nagaraja, S., Wallqvist, A., Reifman, J. & Mitrophanov, A. Y. Computational approach to characterize causative factors and molecular indicators of chronic wound inflammation. *J. Immunol.* **192**, 1824–1834 (2014).
33. Baker, M., Brook, B. S. & Owen, M. R. Mathematical modelling of cytokines, MMPs and fibronectin fragments in osteoarthritic cartilage. *J. Math. Biol.* **75**, 985–1024 (2017).
34. Powell, B., Szleifer, I. & Dhaher, Y. Y. In silico study of principal sex hormone effects on post-injury synovial inflammatory response. *PLoS One* **13**, 1–23 (2018).
35. Marsh, E. E. et al. Estrogen levels are higher across the menstrual cycle in African-American women compared with Caucasian women. *J. Clin. Endocrinol. Metab.* **96**, 3199–3206 (2011).
36. Mumford, S. L. et al. The utility of menstrual cycle length as an indicator of cumulative hormonal exposure. *J. Clin. Endocrinol. Metab.* **97**, E1871–E1879 (2012).
37. Irie, K., Uchiyama, E. & Iwasa, H. Intraarticular inflammatory cytokines in acute anterior cruciate ligament injured knee. *Knee* **10**, 93–96 (2003).
38. Watt, F. E. et al. Acute molecular changes in synovial fluid following human knee injury: Association with early clinical outcomes. *Arthritis Rheumatol.* **68**, 2129–2140 (2016).
39. Haller, J. M. et al. Intraarticular matrix metalloproteinases and aggrecan degradation are elevated after articular fracture. *Clin. Orthop. Relat. Res.* **473**, 3280–3288 (2015).
40. Struglics, A., Larsson, S., Kumahashi, N., Frobell, R. & Lohmander, L. S. Changes in cytokines and aggrecan ARGS neoepitope in synovial fluid and serum and in C-terminal crosslinking telopeptide of type II collagen and N-terminal crosslinking telopeptide of type I collagen in urine over five years after anterior cruciate ligament rupture: An exploratory analysis in the knee anterior cruciate ligament, nonsurgical versus surgical treatment trial. *Arthritis Rheumatol.* **67**, 1816–1825 (2015).
41. van der Kraan, P. M. Differential role of transforming growth factor-beta in an osteoarthritic or a healthy joint. *J. Bone Metab.* **25**, 65 (2018).
42. Tsuchida, A. I. et al. Cytokine profiles in the joint depend on pathology, but are different between synovial fluid, cartilage tissue and cultured chondrocytes. *Arthritis Res. Ther.* **16**, 1–15 (2014).
43. Koh, S. M. et al. Elevated plasma and synovial fluid interleukin-8 and interleukin-18 may be associated with the pathogenesis of knee osteoarthritis. *Knee* **27**, 26–35 (2020).
44. Heard, B. J. et al. Matrix metalloproteinase protein expression profiles cannot distinguish between normal and early osteoarthritic synovial fluid. *BMC Musculoskelet. Disord.* **13** (2012).
45. Fang, M., Wu, X. C. & Huang, W. Raloxifene upregulated mesangial cell MMP-2 activity via ER- β through transcriptional regulation. *Cell Biochem. Biophys.* **67**, 607–613 (2013).
46. Kaplan, D. J., Cuellar, V. G., Jazrawi, L. M. & Strauss, E. J. Biomarker changes in anterior cruciate ligament-deficient knees compared with healthy controls. *Arthroscopy* **33**, 1053–1061 (2017).
47. Jin, D., Liu, R. & Xu, N. Decreased synovial fluid ghrelin level is associated with acute cartilage injury in patients with anterior cruciate ligament tear. *Orthop. J. Sports Med.* **11** (2013).
48. Vandooren, B. et al. Involvement of matrix metalloproteinases and their inhibitors in peripheral synovitis and down-regulation by tumor necrosis factor α blockade in spondylarthropathy. *Arthritis Rheum.* **50**, 2942–2953 (2004).
49. Srikanth, V. K. et al. A meta-analysis of sex differences prevalence, incidence and severity of osteoarthritis. *Osteoarthr. Cartil.* **13**, 769–781 (2005).
50. Stumpff, K., Hadley, M., Corn, K. & Templeton, K. Sex-based reporting of common musculoskeletal conditions. *J. Womens Health* **30**, 689–693 (2021).
51. Wahl, S. M. et al. Transforming growth factor type beta induces monocyte chemotaxis and growth factor production. *Proc. Natl. Acad. Sci.* **84**, 5788–5792 (1987).
52. Pai, R., Ha, H., Kirschenbaum, M. A. & Kamanna, V. S. Role of tumor necrosis factor- α on mesangial cell MCP-1 expression and monocyte migration: Mechanisms mediated by signal transduction. *J. Am. Soc. Nephrol.* **7**, 914–923 (1996).
53. Zhang, X. & Mosser, D. Macrophage activation by endogenous danger signals. *J Pathol* **214**, 161–178 (2008).
54. Li, Y., Zhou, Y., Wang, Y., Crawford, R. & Xiao, Y. Synovial macrophages in cartilage destruction and regeneration—Lessons learnt from osteoarthritis and synovial chondromatosis. *Biomed. Mater. (Bristol)* **17**, (2022).
55. Ismail, H. M., Didangelos, A., Vincent, T. L. & Saklatvala, J. Rapid activation of transforming growth factor β -activated kinase 1 in chondrocytes by phosphorylation and K63-linked polyubiquitination upon injury to animal articular cartilage. *Arthritis Rheumatol.* **69**, 565–575 (2017).
56. Schuster, R., Rockel, J. S., Kapoor, M. & Hinz, B. The inflammatory speech of fibroblasts. *Immunol. Rev.* **302**, 126–146 (2021).
57. Chou, C. H. et al. Synovial cell cross-talk with cartilage plays a major role in the pathogenesis of osteoarthritis. *Sci. Rep.* **10**, (2020).
58. Sanchez-Lopez, E., Coras, R., Torres, A., Lane, N. E. & Guma, M. Synovial inflammation in osteoarthritis progression. *Nat. Rev. Rheumatol.* **18**, 258–275. <https://doi.org/10.1038/s41584-022-00749-9> (2022).
59. Kim-Wang, S. Y. et al. Immune cell profiles in synovial fluid after anterior cruciate ligament and meniscus injuries. *Arthritis Res. Ther.* **23**, (2021).
60. Li, Y.-S., Luo, W., Zhu, S.-A. & Lei, G.-H. T cells in osteoarthritis: Alterations and beyond. *Front. Immunol.* **8**, 356 (2017).
61. Sebag, M., Parry, S. L., Brennan, F. M. & Feldmann, M. Cytokine stimulation of T lymphocytes regulates their capacity to induce monocyte production of tumor necrosis factor- α , but not interleukin-10: Possible relevance to pathophysiology of rheumatoid arthritis. *Eur. J. Immunol.* **27**, 624–632 (1997).
62. Wagner, D. H., Stout, R. D. & Suttles, J. Role of the CD40-CD40 ligand interaction in CD4 $^{+}$ T cell contact-dependent activation of monocyte interleukin-1 synthesis. *Eur. J. Immunol.* **24**, 3148–3154 (1994).
63. Aarvak, T., Chabaud, M., Miossec, P. & Natvig, J. B. IL-17 is produced by some proinflammatory Th1/Th0 cells but not by Th2 cells. *J. Immunol.* **162**, 1246–1251 (1999).
64. Slaughterbeck, J. R. et al. The menstrual cycle, sex hormones, and anterior cruciate ligament injury. *J. Athl. Train.* **37**, 275–278 (2002).
65. Kou, X. X. et al. 17 β -estradiol aggravates temporomandibular joint inflammation through the NF- κ B pathway in ovariectomized rats. *Arthritis Rheum.* **63**, 1888–1897 (2011).

66. Boyan, B. D. et al. Hormonal modulation of connective tissue homeostasis and sex differences in risk for osteoarthritis of the knee. *Biol. Sex Differ.* **4**, 1 (2013).
67. Notbohm, H. L., Umlauft, L., Bloch, W. & Schumann, M. Comparison of the cytokine responses to acute strength exercise between oral contraceptive users and naturally cycling women. *Eur. J. Appl. Physiol.* <https://doi.org/10.1007/s00421-023-05275-4> (2023).
68. Chang, S. J., Kuo, S. M., Lin, Y. T. & Yang, S. W. The biological effects of sex hormones on rabbit articular chondrocytes from different genders. *Biomed. Res. Int.* **2014**, (2014).
69. Bianchi, V. E. The anti-inflammatory effects of testosterone. *J. Endocr. Soc.* **3**, 91–107 (2019).
70. Unemori, E. N., Bair, M. J., Bauer, E. A. & Amento, E. P. Stromelysin expression regulates collagenase activation in human fibroblasts: Dissociable control of two metalloproteinases by interferon- γ . *J. Biol. Chem.* **266**, 23477–23482 (1991).
71. Ogata, Y., Enghild, J. J. & Nagase, H. Matrix metalloproteinase 3 (stromelysin) activates the precursor for the human matrix metalloproteinase 9. *J. Biol. Chem.* **267**, 3581–3584 (1992).
72. Lovering, R. M. & Romani, W. A. Effect of testosterone on the female anterior cruciate ligament. *Am. J. Physiol. Regul. Integr. Comp. Physiol.* **289**, (2005).
73. Garriga, C. et al. Clinical and molecular associations with outcomes at 2 years after acute knee injury: A longitudinal study in the knee injury cohort at the Kennedy (KICK). *Lancet Rheumatol.* **3**, e648–e658 (2021).
74. Bigoni, M. et al. Acute and late changes in intraarticular cytokine levels following anterior cruciate ligament injury. *J. Orthop. Res.* **31**, 315–321 (2013).
75. Marlina, M. et al. Conditioned medium of IGF1-induced synovial membrane mesenchymal stem cells increases chondrogenic and chondroprotective markers in chondrocyte inflammation. *Biosci. Rep.* **41**, (2021).
76. Anderson, J. R. et al. 1H NMR metabolomics identifies underlying inflammatory pathology in osteoarthritis and rheumatoid arthritis synovial joints. *J. Proteome Res.* **17**, 3780–3790 (2018).
77. Kar, S. et al. Modeling IL-1 induced degradation of articular cartilage. *Arch. Biochem. Biophys.* **594**, 37–53 (2016).
78. Meehan, R. T. et al. Synovial fluid cytokines, chemokines and MMP levels in osteoarthritis patients with knee pain display a profile similar to many rheumatoid arthritis patients. *J. Clin. Med.* **10**, 1–14 (2021).
79. Horrigan, L. A., Kelly, J. P. & Connor, T. J. Immunomodulatory effects of caffeine: Friend or foe?. *Pharmacol. Ther.* **111**, 877–892 (2006).
80. Pedersen, B. K. Anti-inflammatory effects of exercise: Role in diabetes and cardiovascular disease. *Eur. J. Clin. Invest.* **47**, 600–611 (2017).
81. Fang, P. K., Ma, X. C., Ma, D. L. & Fu, K. Y. Determination of interleukin-1 receptor antagonist, interleukin-10, and transforming growth factor- β 1 in synovial fluid aspirates of patients with temporomandibular disorders. *J. Oral Maxillofac. Surg.* **57**, 922–928 (1999).
82. Mancini, D. et al. New methodologies to accurately assess circulating active transforming growth factor- β 1 levels: implications for evaluating heart failure and the impact of left ventricular assist devices. *Transl. Res.* **192**, 15–29 (2018).
83. Orlowsky, E. W. & Kraus, V. B. The role of innate immunity in osteoarthritis: When our first line of defense goes on the offensive. *J. Rheumatol.* **42**, 363–371. <https://doi.org/10.3899/jrheum.140382> (2015).
84. Iversen, I. J., Pham, T. M. & Schmal, H. Do acute inflammatory cytokines affect 3- and 12-month postoperative functional outcomes—a prospective cohort study of 12 patients with proximal tibia fractures. *BMC Musculoskelet. Disord.* **22**, (2021).
85. Khalkhali-Ellis, Z. et al. Estrogen and progesterone regulation of human fibroblast-like synoviocyte function in vitro: Implications in rheumatoid arthritis. *J. Rheumatol.* **27**, 1622–1631 (2000).
86. Liang, Y. et al. E2 regulates MMP-13 via targeting miR-140 in IL-1 β -induced extracellular matrix degradation in human chondrocytes. *Arthritis Res. Ther.* **18**, 1–10 (2016).
87. Watt, F. Arthritis in the perimenopause. *Maturitas* **100**, 108 (2017).
88. Cimmino, M. A. & Parodi, M. Risk factors for osteoarthritis. *Semin. Arthritis Rheum.* **34**, 29–34 (2005).
89. Coryell, P. R., Diekman, B. O. & Loeser, R. F. Mechanisms and therapeutic implications of cellular senescence in osteoarthritis. *Nat. Rev. Rheumatol.* **17**, 47–57 (2021).
90. Gulati, M., Dursun, E., Vincent, K. & Watt, F. E. The influence of sex hormones on musculoskeletal pain and osteoarthritis. *Lancet Rheumatol.* **5**, e225–e238 (2023).
91. Italiani, P. & Boraschi, D. From monocytes to M1/M2 macrophages: Phenotypical vs. functional differentiation. *Front. Immunol.* **5**, 1–22 (2014).
92. Byrne, A. & Reen, D. J. Lipopolysaccharide induces rapid production of IL-10 by monocytes in the presence of apoptotic neutrophils. *J. Immunol.* **168**, 1968–1977 (2002).
93. Huang, T. L., Hsu, H. C., Yang, K. C. & Lin, F. H. Hyaluronan up-regulates IL-10 expression in fibroblast-like synoviocytes from patients with tibia plateau fracture. *J. Orthop. Res.* **29**, 495–500 (2011).
94. Müller, R. D. et al. IL-10 overexpression differentially affects cartilage matrix gene expression in response to TNF- α in human articular chondrocytes in vitro. *44*, 377–385 (2008).
95. Parker, E. et al. Low oxygen tension increased fibronectin fragment induced catabolic activities-response prevented with biomechanical signals. *Arthritis Res. Ther.* **15**, 1–12 (2013).
96. Smythies, L. E. et al. Human intestinal macrophages display profound inflammatory anergy despite avid phagocytic and bacteriocidal activity. *J. Clin. Investig.* **115**, 66–75 (2005).
97. Inoue, H. et al. An investigation of cell proliferation and soluble mediators induced by interleukin 1beta in human synovial fibroblasts: Comparative response in osteoarthritis and rheumatoid arthritis. *Inflamm. Res.* **50**, 65–72 (2001).
98. Russell, R. E. K. et al. Release and activity of matrix metalloproteinase-9 and tissue inhibitor of metalloproteinase-1 by alveolar macrophages from patients with chronic obstructive pulmonary disease. *Am. J. Respir. Cell Mol. Biol.* **26** www.atsjournals.org (2002).
99. Asano, K. et al. Suppression of matrix metalloproteinase production from synovial fibroblasts by meloxicam in-vitro. *J. Pharm. Pharmacol.* **58**, 359–366 (2010).
100. Cha, H. S. et al. Influence of hypoxia on the expression of matrix metalloproteinase-1, -3 and tissue inhibitor of metalloproteinase-1 in rheumatoid synovial fibroblasts. *Clin. Exp. Rheumatol.* **21**, 593–598 (2003).
101. Rankin, K. S. et al. A Novel in vitro model to investigate behavior of articular chondrocytes in osteoarthritis. *J. Rheumatol.* **37**, 426–431 (2010).
102. Jager, N. A. et al. Distribution of matrix metalloproteinases in human atherosclerotic carotid plaques and their production by smooth muscle cells and macrophage subsets. *Mol. Imaging Biol.* **18**, 283–291 (2016).
103. Hashizume, M. & Miura, M. High molecular weight hyaluronic acid inhibits IL-6-induced MMP production from human chondrocytes by up-regulating the ERK inhibitor, MKP-1. *Biochem. Biophys. Res. Commun.* **403**, 184–189 (2010).
104. Wu, D.-Q., Zhong, H., Ding, Q. & Ba, L. Protective effects of biochanin A on articular cartilage: in vitro and in vivo studies. *BMC Complement. Altern. Med.* **14**, 444 (2014).
105. Fuchs, S., Skwara, A., Bloch, M. & Dankbar, B. Differential induction and regulation of matrix metalloproteinases in osteoarthritic tissue and fluid synovial fibroblasts. *12*, 409–418 (2004).
106. Thomassen, M. J., Divis, L. T. & Fisher, C. J. Regulation of human alveolar macrophage inflammatory cytokine production by interleukin-10. *Clin. Immunol. Immunopathol.* **80**, 321–324 (1996).

107. Fu, Y., Lei, J., Zhuang, Y., Zhang, K. & Lu, D. Overexpression of HMGB1 A-box reduced IL-1 β -induced MMP expression and the production of inflammatory mediators in human chondrocytes. *Exp. Cell Res.* **349**, 184–190 (2016).
108. Dunn, S. L., Wilkinson, J. M., Crawford, A., Le Maitre, C. L. & Bunning, R. A. D. Cannabinoid WIN-55,212-2 mesylate inhibits interleukin-1 β induced matrix metalloproteinase and tissue inhibitor of matrix metalloproteinase expression in human chondrocytes. *Osteoarthr. Cartil.* **22**, 133–144 (2014).
109. Kothari, P. et al. IL-6-mediated induction of matrix metalloproteinase-9 is modulated by JAK-dependent IL-10 expression in macrophages. *J. Immunol.* **192**, 349–357 (2014).
110. Schindler, R. et al. Correlations and interactions in the production of interleukin-6 (IL-6), IL-1, and tumor necrosis factor (TNF) in human blood mononuclear cells: IL-6 suppresses IL-1 and TNF. *Blood* **75**, 40–47 (1990).
111. Kaneva, M. K. et al. Chondroprotective and anti-inflammatory role of melanocortin peptides in TNF- α activated human C-20/A4 chondrocytes. *Br. J. Pharmacol.* **167**, 67–79 (2012).
112. Calippe, B. et al. 17 β -estradiol promotes TLR4-triggered proinflammatory mediator production through direct estrogen receptor α signaling in macrophages *in vivo*. *J. Immunol.* **185**, 1169–1176 (2010).
113. Agostino, P. et al. Sex hormones modulate inflammatory mediators produced by macrophages. *Ann. N. Y. Acad. Sci.* **876**, 426–429 (1999).
114. Liu, L. et al. Estrogen inhibits LPS-induced IL-6 production in macrophages partially via the nongenomic pathway. *Immunol. Invest.* **43**, 693–704 (2014).
115. Sun, Y. et al. miR-155 mediates suppressive effect of progesterone on TLR3, TLR4-triggered immune response. *Immunol. Lett.* **146**, 25–30 (2012).
116. Oettel, M. & Mukhopadhyay, A. K. Progesterone: The forgotten hormone in men?. *Aging Male* **7**, 236–257 (2004).
117. Cooke, P. S., Nanjappa, M. K., Ko, C., Prins, G. S. & Hess, R. A. Estrogens in male physiology. *Physiol. Rev.* **97**, 995–1043 (2017).
118. McKay, M. D., Beckman, R. J. & Conover, W. J. Comparison of three methods for selecting values of input variables in the analysis of output from a computer code. *Technometrics* **21**, 239–245 (1979).
119. Saltelli, A., Chan, K. & Scott, E. M. *Sensitivity Analysis*. vol. 134 (2000).
120. Sobol', I. M. Global sensitivity indices for nonlinear mathematical models and their Monte Carlo estimates. *Math. Comput. Simul.* **55**, 271–280 (2001).
121. Pianosi, F., Sarrazin, F. & Wagener, T. A Matlab toolbox for global sensitivity analysis. *Environ. Model. Softw.* **70**, 80–85 (2015).
122. Bilal, N. Implementation of Sobol's method of global sensitivity analysis to a compressor simulation model. In: *22nd International Compressor Engineering Conference at Purdue* 1–10 (2014).
123. Olmayan, P. et al. The methods used in nonparametric covariance analysis. *Duzce Med. J.* **20** www.masungur.com/nancova0.php (2018).

Acknowledgements

We want to thank Subaryani Soedirdjo for assisting in MATLAB programming, and Dr. Nancy Monson from UT Southwestern Medical Center for her contributions on providing insights into immune cell inclusion into this model. This work was supported in part by the UT Southwestern Cain Endowment (YYD), and by the National Institute of Arthritis and Musculoskeletal and Skin Diseases (1R01AR069176-01A1) (YYD).

Author contributions

Conceptualization: C.H., B.L., Y.Y.D. Data acquisition: C.H. Data analysis: C.H., K.K. Supervision: C.H., B.L., Y.Y.D. Data interpretation: C.H., B.L., Y.Y.D. All authors contributed to writing and approving the manuscript for publication.

Funding

Funding was provided by National Institute of Arthritis and Musculoskeletal and Skin Diseases (Grant No. 1R01AR069176-01A1).

Declarations

Competing interests

The authors declare no competing interests.

Additional information

Supplementary Information The online version contains supplementary material available at <https://doi.org/10.1038/s41598-024-77730-x>.

Correspondence and requests for materials should be addressed to Y.Y.D.

Reprints and permissions information is available at www.nature.com/reprints.

Publisher's note Springer Nature remains neutral with regard to jurisdictional claims in published maps and institutional affiliations.

Open Access This article is licensed under a Creative Commons Attribution-NonCommercial-NoDerivatives 4.0 International License, which permits any non-commercial use, sharing, distribution and reproduction in any medium or format, as long as you give appropriate credit to the original author(s) and the source, provide a link to the Creative Commons licence, and indicate if you modified the licensed material. You do not have permission under this licence to share adapted material derived from this article or parts of it. The images or other third party material in this article are included in the article's Creative Commons licence, unless indicated otherwise in a credit line to the material. If material is not included in the article's Creative Commons licence and your intended use is not permitted by statutory regulation or exceeds the permitted use, you will need to obtain permission directly from the copyright holder. To view a copy of this licence, visit <http://creativecommons.org/licenses/by-nc-nd/4.0/>.

© The Author(s) 2024